# Discretization of small-scale, stratigraphic heterogeneities and its impact on the seismic response

## Lessons from the application of process-based modelling

Cuesta Cano, Andrea; Karimzadanzabi, Azin; Storms, Joep Elisabeth Anton; Rongier, Guillaume; Verschuur, Dirk Jacob; Martinius, Allard Willem

**DOI**
10.1111/1365-2478.70015

**Publication date**
2025

**Document Version**
Final published version

**Published in**
Geophysical Prospecting

**Citation (APA)**
Cuesta Cano, A., Karimzadanzabi, A., Storms, J. E. A., Rongier, G., Verschuur, D. J., & Martinius, A. W. (2025). Discretization of small-scale, stratigraphic heterogeneities and its impact on the seismic response: Lessons from the application of process-based modelling. *Geophysical Prospecting*, *73*(4), 1280-1300. https://doi.org/10.1111/1365-2478.70015

Received: 14 November 2024 | Accepted: 22 February 2025

DOI: 10.1111/1365-2478.70015

Geophysical Prospecting | EAGE EUROPEAN ASSOCIATION OF GEOSCIENTISTS & ENGINEERS

ORIGINAL ARTICLE

# Discretization of small-scale, stratigraphic heterogeneities and its impact on the seismic response: Lessons from the application of process-based modelling

**Andrea Cuesta Cano**[1] | **Azin Karimzadanzabi**[1] | **Joep Elisabeth Anton Storms**[1] | **Guillaume Rongier**[1] | **Dirk Jacob Verschuur**[1] | **Allard Willem Martinius**[1,2]

[1]Department of Geoscience & Engineering, TU Delft, Delft, The Netherlands

[2]Equinor Research Center, Equinor S.A., Trondheim, Norway

**Correspondence**
Andrea Cuesta Cano, Department of Geoscience & Engineering, TU Delft, Delft, The Netherlands. Email: A.CuestaCano@tudelft.nl

## Abstract

Reducing the uncertainty of reservoir characterization requires to better identify the small-scale structures of the subsurface from the available data. Studying the seismic response of meter-scale, stratigraphic heterogeneities typically relies on the generation of reservoir models based on outcrop examples and their forward seismic modelling. To bridge geological information and seismic modelling, these methods allocate values of acoustic properties, such as mass-density and P-wave velocity, according to discretized properties like layer-type lithology or facies units. This strategy matches the current workflow in seismic data inversion in industry, where modelling workflows are based on lithofacies distributions. However, from stratigraphic modelling, we know that meter-scale heterogeneities occur within certain facies and lithologies. Here, we evaluate the difference on the seismic response between allocating acoustic properties in a grain size–based, semi-continuous manner versus discretized manners based on lithology and facies classifications. To do so, we generate a reference geological simulation that we populate with acoustic properties, mass-density and P-wave velocity, using three different strategies: (1) based on grain size distribution; (2) based on facies distribution; and (3) based on lithology. The method we propose includes the generation of realistic geological simulations based on stratigraphic modelling and the transformation of its output into acoustic properties, honouring the intra-lithology and intra-facies, small-scale structures. We, then, generate seismic data by applying a forward seismic modelling workflow. The synthetic data show that the grain size–based simulation allows the identification of small-scale, stratigraphic heterogeneities, such as beds with strong density and velocity contrasts. These stratigraphic structures are smoothened or may completely disappear in the facies and lithology discretized simulations and, therefore, are not (well) represented in the synthetic seismic data. Recognizing meter-scale, stratigraphic heterogeneities is relevant for the characterization of the fluid flow in the reservoir. However, current discrete and lithology-based strategies in seismic inversion

are not able to resolve such heterogeneities because real subsurface properties are not discrete properties but continuous, unless there are stratigraphic discontinuities such as erosional surfaces or faults. This research works towards a better understanding of the relationship between changes in these continuous properties and the observed seismic data by introducing greater complexity into the discretized geological simulations. Here, we use synthetic seismic images with the goal of eventually aiding in fine-tuning seismic inversion methodologies applied to real seismic data. One pathway is to foster the development of inversion approaches that can leverage stratigraphic modelling to get stronger geological priors and replace the standard but inadequate multi-Gaussian prior.

**KEYWORDS**
imaging, interpretation, petrophysics, reservoir geophysics, seismics

## INTRODUCTION

Understanding multiscale, spatial sedimentary and stratigraphic architecture of reservoirs and the variability of associated discrete and continuous properties is crucial for the advancement of subsurface projects, such as storing $CO_2$ or $H_2$, groundwater or exploring for mineral resources (de Jager, 2021; Simmons et al., 2023). One of main techniques to study the subsurface and the structures herein is seismic reflection data acquisition. The resolution of seismic data is controlled by two main factors that define the size of the observable structures: the frequency of acquisition and the depth of the reservoir to be characterized (Yilmaz, 2001). Under perfect conditions, the vertical resolution is one fourth of the wavelength, which depends on the average velocity of the rocks and the acquisition frequency. However, the wavelength increases with depth due to attenuation processes, which means that the vertical resolution decreases (Cox et al., 2020; Yilmaz, 2001). The lateral resolution is also a function of depth and wavelength (Chopra et al., 2006; Cox et al., 2020). Considering that stratigraphic heterogeneities, both discrete and continuous, occur at spatial scales ranging from millimetres to 10th of meters, heterogeneities will be present below the vertical seismic resolution (Jackson et al., 2019; Klausen et al., 2018; Zeng et al., 2013). Examples of discrete heterogeneities include channels encased in fine-grained deposits or the stacking of different depositional facies (a facies is a rock type deposited under particular environmental conditions and that, therefore, has similar lithological characteristics such as a gradational porosity change). Examples of continuous heterogeneities, and the focus of this paper, include gradual changes in grain size distribution and, thus, porosity. These features cannot always be interpreted on seismic reflection data, even though they affect subsurface fluid flow (Howell et al., 2008; Jackson et al., 2009; Ringrose & Bentley, 2015; Sech et al., 2009).

Seismic forward modelling tools have been used to better understand the seismic response of meter-scale, stratigraphic heterogeneities that are close to the resolution limits of seismic data (Anell et al., 2016; Bakke et al., 2008; Bakke et al., 2013; Hodgetts & Howell, 2000; Rabbel et al., 2018; Shuster & Aigner, 1994; Tomasso et al., 2010; Wan et al., 2022). These studies mainly focus on analysing the seismic response of heterogeneities of deep-water channel and lobe deposits (Armitage & Stright, 2010; Jackson et al., 2019; Pemberton et al., 2018) and deltaic clinoform geometries (Grasseau et al., 2019; Holgate et al., 2014; Holgate et al., 2015; Zeng et al., 2013). The typical workflow combines collecting outcrop data (architecture, lithology and/or facies) for the purpose of creating a geological model of the outcrop and, subsequently, converting this model into synthetic seismograms, often deploying different seismic frequencies (Armitage & Stright, 2010; Bakke et al., 2013; Feng et al., 2017; Grasseau et al., 2019; Pemberton et al., 2018). Thereafter, the outcrop-based synthetic seismic model is used to inform and improve the construction of a subsurface reservoir model.

An essential step in forward seismic modelling is to populate a geological reservoir model with petrophysical and acoustic properties (mass-density and P-wave velocity). In addition, S-wave velocity also needs to be defined in the case of full elastic seismic modelling. Most commonly, those properties come from measurements in the borehole and from core plugs (Bakke et al., 2013; Bourgeois et al., 2004; Falivene et al., 2010; Grippa et al., 2019; Hodgetts & Howell, 2000; Rabbel et al., 2018). Other studies developed and applied experimental equations that relate shale volume, density, porosity or clay content to calculate acoustic properties (Armitage & Stright, 2010; Eberhart-Phillips et al., 1989; Feng et al., 2017; Han et al., 1986; Shuster & Aigner, 1994). No matter whether core or experimental data are used, these studies allocate only one value of each property to all the cells of the model with the same lithology or facies (Bakke

et al., 2013; Feng et al., 2017; Grippa et al., 2019; Hodgetts & Howell, 2000; Pemberton et al., 2018). The allocation of single values matches with the workflows applied in seismic data inversion, where constant values are used to simplify geological modelling (Barajas-Olalde et al., 2021; Cardiff & Kitanidis, 2009; Kemper & Gunning, 2014; Pendrel & Schouten, 2020).

However, relying upon outcrop data and the allocation of single property values per lithology or facies for the analysis of small-scale heterogeneities poses two challenges. First, the number of good-quality outcrops, laterally extensive and that allow 3D observation, is limited, and so it is the variability of heterogeneities that is represented on them. And second, continuous sedimentological and petrophysical properties, such as grain size or porosity, vary within the same lithology and facies (Howell et al., 2008). Therefore, allocating a single-property value to individual lithology/facies might not honour the internal variability within certain facies and lithologies.

This paper evaluates the impact on the seismic response of allocating petrophysical and acoustic properties based on a continuous property, such as grain size, and, consequently, considering the internal variations within different facies and lithologies. We compare the results to the seismic response that allocating the properties based on lithology and facies produces. Using lithology and facies represents coarser discretization levels and, as previously mentioned, is the common strategy to populate geological models. For this purpose, we have designed a method that does not depend on outcrop data for the generation of the geological models but on stratigraphic modelling tools and that handles the allocation of petrophysical and acoustic properties beyond lithology/facies resolution and based on grain size distribution.

We focus on meter-scale heterogeneities, here referred to as small-scale heterogeneities, present in a 2D simulation of a wave-dominated shallow marine system. Wave-dominated shallow marine systems are characterized by clean sand and gravel, often well sorted and abraded (Roy et al., 1995), and have been targeted in the subsurface because of their promising reservoir potential (Bhattacharya & Walker, 1991; Lis & Wysocka, 2012; Tahir et al., 2018; Tyler & Finley, 1991). Meter-scale heterogeneities in wave-dominated systems are associated with (1) erosional surfaces and abrupt or gradual transitions between diverse lithologies (Hampson & Storms, 2003), and (2) gradual rock property changes, including porosity (Ketzer et al., 2002; Sømme et al., 2008; Taylor et al., 2000). The formation of such heterogeneities and the processes of deposition, transport and erosion that control their formation are understood and can be predicted, as they are based on sedimentological processes that were previously studied. In the case of wave-dominated shoreface environments, we refer to Anthony (2013), Anthony and Aagaard (2020) and Mitchell and Zhao (2023), Backstrom et al. (2015), Field and Roy (1984), Keen et al. (2012), Kumar and Sanders (1976), Madsen (1991), Swift et al. (1991). This knowledge is the basis for focused stratigraphic modelling tools that simulate the sedimentological processes to generate synthetic stratigraphy. Some of these tools also include the modelling of processes from wave-dominated shoreface environments (Laigle et al., 2013; Paola, 2000; Quiquerez et al., 2004; Storms, 2003; Storms et al., 2002; Tetzlaff, 2005). For our research, we base the stratigraphic modelling on the tool presented by Storms et al. (2002).

Stratigraphic modelling tools have been previously used in combination with forward stratigraphic modelling to evaluate the influence of sedimentary processes at basin and sub-basin scale (Granjeon, 2019; Wan et al., 2022). In this paper, though, we apply a similar methodology to explore the impact on the seismic response of assigning acoustic properties based on different levels of discretization. To do so, we define a workflow based on stratigraphic forward modelling to create a synthetic geological simulation, at a cell size of $2 \times 2$ m$^2$, that we will use as reference model for our research. Each cell includes information about grain size, facies and lithology. These three data types are used to generate three different scenarios, where the distribution of acoustic properties, mass-density and P-wave velocity depends on different data types. The distribution based on grain size includes the greater level of detail, whereas the lithology-based represents the greatest discretization level. By applying numerical seismic modelling and inversion, we obtain synthetic seismic data for each scenario. The observations on the seismic data demonstrate that some of the stratigraphic heterogeneities of our simulation can still be observed in the grain size–based scenario, whereas they are vaguely represented or even erased for the lithology- and facies-based discretization scenarios.

## METHODOLOGY: FROM STRATIGRAPHIC MODELLING TO SYNTHETIC SEISMIC DATA

Because we limit ourselves to wave-dominated shoreface models, we can assume our geologic structures to have a so-called 2.5D characteristic, meaning that we do not expect large variations in the along-shore direction. Therefore, we can limit our studies to 2D cross-sections of the models. In addition, this paper aims to demonstrate the effect of transferring the detailed geologic models to a discretized version suitable for seismic data analysis. Although the Earth—of course—is an elastic medium, we limit ourselves to the recording of P-wave data via a water layer that is put on top of our subsurface models. In addition, we mainly look at the structural seismic images; therefore, we can limit ourselves to acoustic seismic data modelling, neglecting the effect of S-wave velocity variations as well as S-waves in the seismic measurements.

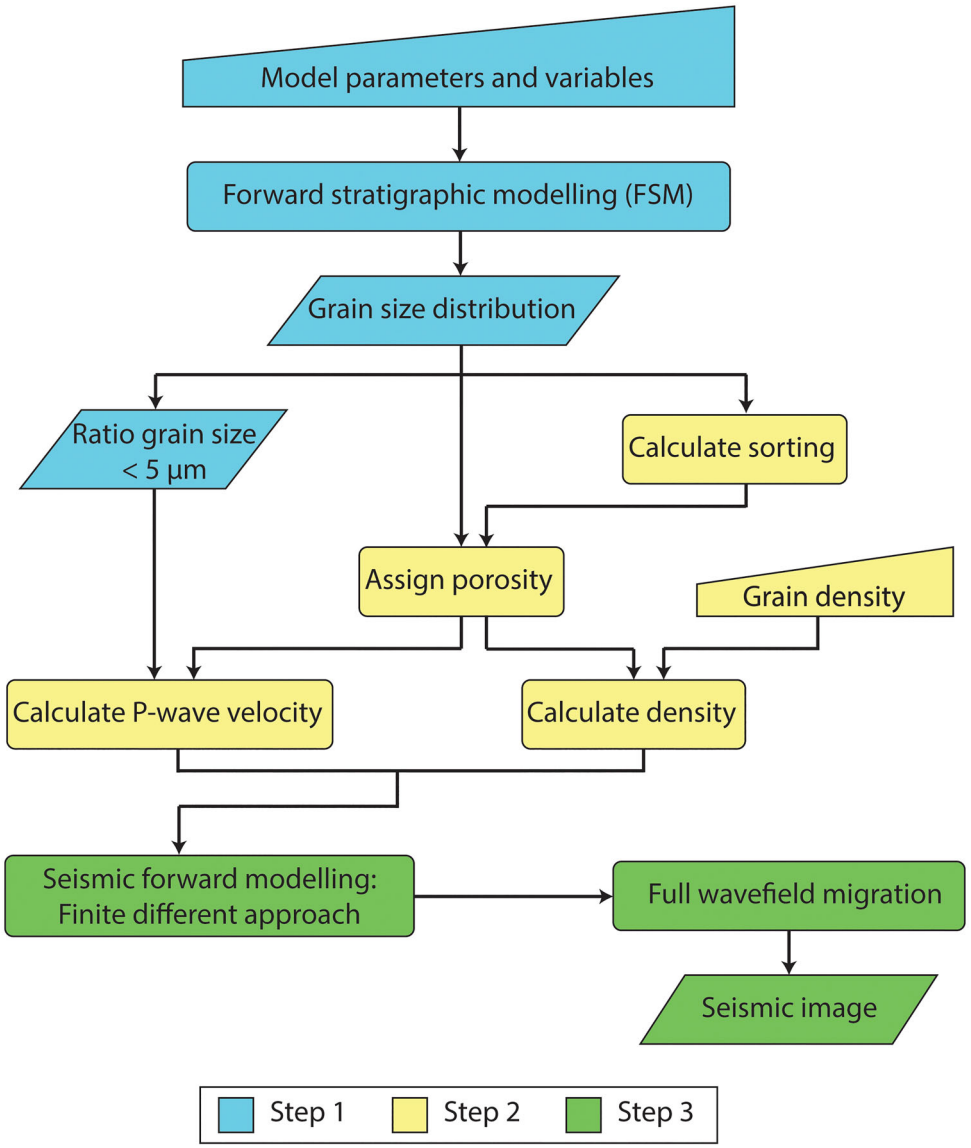


**FIGURE 1** Methodology to generate the synthetic seismic data, composed of three steps. Step 1 (blue) is the generation of geological simulations. Step 2 (yellow) is the processes to populate the simulations with acoustic parameters—mass-density and P-wave velocity—based on grain size distribution. Step 3 (green) consists of the application of seismic forward modelling techniques and migration to obtain the seismic subsurface image. The final output is the seismic image.

The method we apply to evaluate the impact on the seismic data of the discretization of small-scale, stratigraphic heterogeneities is based on three steps (Figure 1). The first step is the use of a stratigraphic modelling tool to create a 2D geological simulation that includes architectural features at different scales. The output includes grain size distribution (ratio of every grain size class and mean grain size), lithology and facies data for each grid cell. The second step consists of converting the grain size distribution data into acoustic parameters—mass-density and P-wave velocity. Finally, we perform seismic forward modelling followed by migration to generate a structural seismic image. Because we sum the contribution of all angles into a single structural image, angle-dependent imaging is not directly highlighted.

## Step 1: Generation of geological simulations using stratigraphic modelling tools

Forward stratigraphic modelling (FSM) mimics the processes of erosion and deposition we observe in nature to distribute sediment and create synthetic stratigraphic architectures. Compared to other modelling tools (see Pyrcz et al., 2015 for more details on this topic), FSM has two main advantages: (1) It mimics the rules of physics and hydrodynamics

that result in patterns of deposition that follow Walthers' law. (2) It deals with the issue of preservation potential, where erosion will remove part of the strata in a predictable manner.

There are many different FSM tools available with various degrees of complexity and accessibility (Pyrcz et al., 2015). For this study, we defined three requirements that the FSM tool must meet. First, the FSM tool must be able to simulate the formation of sedimentary heterogeneities at meter scale, in the vertical direction, and in the order of tens of meters in the horizontal direction. Second, the FSM tool must have a low computational cost, allowing the generation of several scenarios within limited run-time on a laptop/desktop machine. Third, the FSM tool should provide grain size distribution data or sediment grain size proportion as output because the acoustic property allocation procedure is based on grain size, as explained in the following subsection. Preferably, the FSM tool should also be open-source so the code can be adapted to fit the workflow.

BarSim, a process–response approach that simulates the long-term coastal evolution and stratigraphic architecture through time of wave-dominated coastal systems (Storms, 2003; Storms & Swift, 2003; Storms et al., 2002), meets all those requirements. This model is based on a simple approximation of a 2D cross-shore profile and simulates the deposition of individual storm beds, with thickness values that go down to the centimetre scale (Storms, 2003; Storms & Swift, 2003). BarSim applies mass conservation principles to erosion, transport and deposition of multiple grain size classes along a 2D profile at surface conditions (Charvin et al., 2011; Storms, 2003; Storms & Swift, 2003). This means that sediment that is eroded at any location on the shoreface due to the action of waves is transported and deposited at other locations in the 2D profile, where accommodation is available. Sediment input into and out of the model occurs as along-shore transport, which is defined as net sediment input by the user (Charvin et al., 2011).

The input variables are as follows: (1) model parameters controlling sediment erosion, transport and deposition (wave efficiency, rate of erosion, characteristic travel distances); (2) time-dependent variables (sea level, sediment budget); and (3) variables that define the base conditions (grain size distributions, littoral drift, wave-base depth, substrate slope) (Storms et al., 2002). The time-dependent variables and the variables that define the base conditions of the model can be modified to create a variety of outputs. The output includes sedimentological information (fraction of the different grain size classes, mean grain size, sorting, facies) for all the grid cells (Storms & Hampson, 2005).

We use an implementation of BarSim, called pyBarSim, to generate the geological simulations (Rongier et al., 2023). pyBarsim is a recently developed Python package, which speeds up the simulation process. This package also allows the interpolation of the simulated sediment layers onto a regular grid.

For this study, lithology is derived from the grain size distributions. To do so, we assume that the simulation is solely composed of quartz grains. The cells are labelled siltstone or sandstone based on the proportion of the different grain size classes. For our set-up, when the grain size classes corresponding to 5 and 50 μm show a proportion of 50% or higher, the cell is identified as siltstone (Merriman et al., 2003; Picard, 1971; Schön, 2011). The cells for which the proportion is under 50% are defined as sandstone.

At the end of this step, every cell of the grid has three associated properties: grain size distribution (as a proportion of each grain size class), facies (as a label) and lithology (as a label).

## Step 2: Population of acoustic property values

From the geological simulations, we obtain, for each cell, grain size distributions at surface conditions. In Step 2, we will transform that data into acoustic properties (mass-density and P-wave velocity) at certain depths. During this transformation, we will use intermediate parameters, such as sorting, initial porosity and final porosity.

First, the sorting is calculated as a weighted standard deviation of the grain size distribution. Then, we use the relationships from Friedman (1962) to convert the sorting parameter from standard deviation to Trask coefficients (Trask 1930). With mean grain size and sorting distribution, we can assign initial porosity, following empirical relationships described in literature (Beard & Weyl, 1973; Folk & Ward, 1957; Rogers & Head, 1961; Wendebourg & Harbaugh, 1997). To do so, we apply an interpolation to each cell based on the relationship among initial porosity, mean grain size and sorting reported by Beard and Weyl (1973) for wet, unconsolidated mixtures. Lastly, we define the overburden and calculate the final porosity. To calculate the final porosity, a porosity loss function is applied, following the trends defined in the look-up table from SedSim (Tetzlaff, 2005; Tetzlaff & Harbaugh, 1989) based on Wendebourg and Harbaugh (1997).

Once the final porosity value is obtained, density is calculated under two assumptions: (1) The grains are pure quartz. (2) The porosity is water-saturated. For the calculation of P-wave velocity, the empirical equation proposed by Eberhart-Philips et al. (1989) is used:

$$V_P = 5.77 + 6.94\phi - 1.73\sqrt{C} + 0.446\left(P_e - e^{-16.7P_e}\right), \quad (1)$$

where $\phi$ is porosity (dimensionless), $C$ is clay content (dimensionless) and $P_e$ is effective pressure (kbar). The resulting P-wave velocity is in km/s. The clay content is directly

obtained from the grain size distribution produced by pyBarSim. The effective pressure is user-defined, and it must match the characteristics of the applied overburden.

Following this method, we can create simulations where the acoustic properties are derived from grain size distribution. To populate the facies- and lithology-based simulations, we extract the acoustic property values for each facies/lithology class, and we calculate the average. The resulting average value is, then, assigned to all the cells with the same label. This way, we ensure that the values from the grain size–based, facies-based and lithology-based simulations are related to each other.

## Step 3: Forward seismic modelling and migration

### Forward seismic modelling: finite difference approach

Using geological models that capture the physical properties of the subsurface to replicate seismic field experiments is known as forward numerical modelling of seismic data. Several forward modelling techniques are available, and choosing one is based on a balance between model complexity, accuracy and computing time. Two of the most popular approaches are the ray and wave equation methods. Ray methods rely on the decomposition of the seismic wavefield into independent elementary waves that propagate along rays (Červený et al., 2007). The rays are resolved individually, which simplifies the calculations. Ray tracing methods provide solutions that are accurate within a localized region or along specific ray paths, rather than globally across the entire model. Consequently, ray methods struggle to handle strong and small-scale velocity variation in the medium (Červený, 2001; Rawlinson et al., 2008; Wang et al., 2004). Wave equations do not have the same limitation, as they approach the propagation problem over the entire model as a numerical solution of partial differential equations (Liu & Sen, 2009; Rawlinson et al., 2008). Therefore, wave equations are able to resolve accurate travel-times and amplitudes even in complex media (Rawlinson et al., 2008).

Within wave propagation approaches, the finite difference, time-domain method is a robust numerical approach with a strong ability to model seismograms even in complex and heterogeneous media (Holberg et al., 1990). This method is used to create the synthetic seismograms for this paper due to the stratigraphical complexity that the simulations display. Finite difference techniques can incorporate all wave phenomena, including multiples and diffractions, and they offer precise numerical solutions (Fagin, 1991). The only constraint on finite difference methods is the computing time (Kelly et al., 1976).

In finite difference techniques, seismic wave equations are represented as partial differential equations with spatial and temporal derivatives that are used to explain seismic wave propagation in the subsurface. As an example, one-dimensional acoustic wave propagation is represented by

$$\frac{\partial^2 p(x,t)}{\partial x^2} = \frac{1}{v^2}\frac{\partial^2 p(x,t)}{\partial t^2}, \tag{2}$$

where $p$ and $v$ are wavefield pressure and propagation velocity, respectively, $x$ is distance and $t$ is time. To calculate temporal derivatives, one often uses the second-order finite difference. In addition, by considering the pressure wavefield to be a function of grid size and time step, respectively, as shown by $\Delta x$ and $\Delta t$, the equation expands as follows:

$$\frac{\partial^2 p(x,t)}{\partial t^2} = \lim_{\tau \to 0} \frac{p_{j,m-1} - 2p_{j,m} + p_{j,m+1}}{\Delta t^2}, \tag{3}$$

where $j$ and $m$ represent grid number in both directions, such that $p_{j,m} \equiv p(j\Delta x, m\Delta t)$.

For a spatial derivative, which will require the wavefield values at the current grid cell and its two neighbouring cells, at a given time step, an equation akin to Equation (3) can also be constructed. A graphical representation of such a scenario can be found in Liu and Sen (2009). We can create a recursion formula for solving the 1D wave equation by inserting Equation (3) into Equation (2) and substituting a (2N)th-order finite difference formula for the second-order spatial derivative and rearranging that to

$$p_{j,m+1} = 2p_{j,m} - p_{j,m-1} + \frac{\Delta t^2 v^2}{\Delta x^2} \left[ c_0 p_{j,m} + \sum_{n=1}^{N} C_n \left( p_{j-n,m} + p_{j+n,m} \right) \right]. \tag{4}$$

The wave field values at two successive time steps, $t = 0$ and $t = \Delta t$, are known at the start of the recursion. The final equation (Equation 4) is used to calculate the wavefield values at each spatial location at a future time step. After the calculation of the wavefield, values at each spatial location for a future time step, the finite difference time-domain (FDTD) method continues iteratively, advancing the solution through time to simulate the entire seismic wave propagation ($p_{j,m}$).

Note that for the FDTD modelling in this paper, we use the 2D acoustic wave equation, where pressure is a function of space and depth, and also density variations are taken into account. In FDTD, receivers are strategically placed within the model to capture the seismic wavefield at specific locations as the waves propagate through the subsurface. These receivers record the time-dependent wavefield values, which are used to construct synthetic seismograms.

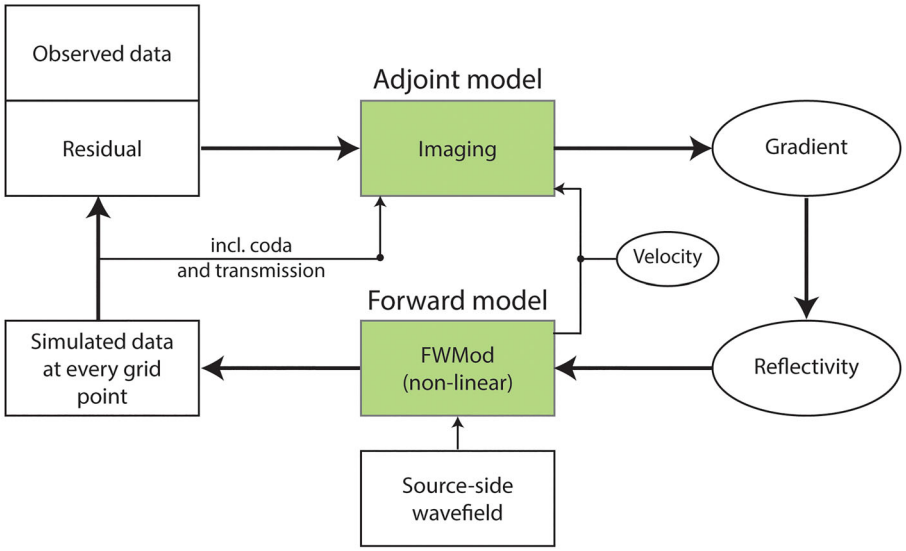


**FIGURE 2** Schematic representation of the full-wavefield migration method. *Source*: Adapted from Davydenko (2016).

### Full-wavefield migration in angle-dependent mode

In the following step, the output from the seismic modelling is migrated to construct the final reflectivity image. Figure 2 represents the block diagram for the full-wavefield migration (FWM) that we apply here following Davydenko and Verschuur (2017). This inversion scheme consists of different blocks of data comparison, adjoint forward model, model update and the forward operator. In the data comparison, the modelled data and the measured data are being compared. In the adjoint forward model, this procedure translates the residual from the data domain to the model domain and generates the model update. In the next block of model update, the model space is refreshed by scaling the update computed in the previous step and adding it to the current model. Finally, the forward model computes new data using the updated model space, which is then used for the subsequent iteration of data comparison (Davydenko & Verschuur, 2017).

The primary feature of this FWM method is its forward model, which generates comprehensive reflection data (Berkhout, 2014). This imaging process benefits from the inversion-based approach. Additionally, its forward model can incorporate angle-dependent reflection information. To achieve such goal, the imaging at each depth level should be carried out in angle-dependent mode: For every lateral location, the down-going wavefield should be cross-correlated with a back-propagated residual that is shifted in space by several spatial lags, creating a spatial reflectivity operator for each grid point in the image domain. Subsequently, a 2D Radon transformation is applied to each reflectivity operator, decomposing the spatial reflectivity operator into reflection properties per angle of incidence. After the FWM-angle dependency generates the image-angle gathers for all lateral locations, the information is summed along the angle axis. This results in a structural reflectivity image created from all angles of incidence, thereby enhancing the overall image information (Davydenko & Verschuur, 2017). Such a method differs from the conventional FWM, which does not leverage spatial lag and Radon transformation and results in the final image primarily reflecting information from normal incidents (Davydenko & Verschuur, 2017).

## MODELLING

### Reference geological simulation

We perform the forward stratigraphic modelling (FSM) using pyBarSim to generate a 2D reference geological simulation that will be used throughout this study. This simulation records the sedimentation and synthetic stratigraphy for a system with four grain size classes (250, 125, 50, 5 μm) and that experiences a relative sea level fall, rise and fall. Supporting Material 1 includes all the values used for the input parameters. The simulation results in a target structure that is 40,000-m long and 200-m thick. The grid cell is $2 \times 2$ m$^2$ to capture the stratigraphic heterogeneities within each facies and lithology. We added 100 m of underburden and 1100 m of overburden, including a 100-m-thick seawater layer on top. Cells have been added to each side of the simulation, equivalent to 2500 m in each case, to ensure adequate illumination of every part of the target area during the forward seismic modelling.

The output of the FSM includes facies distribution (Figure 3a), grain size distribution (in Figure 3b represented as mean grain size) and lithology distribution (Figure 3c), all of them including only part of the overburden. Within the facies distribution (Figure 3a), we identify six different facies based

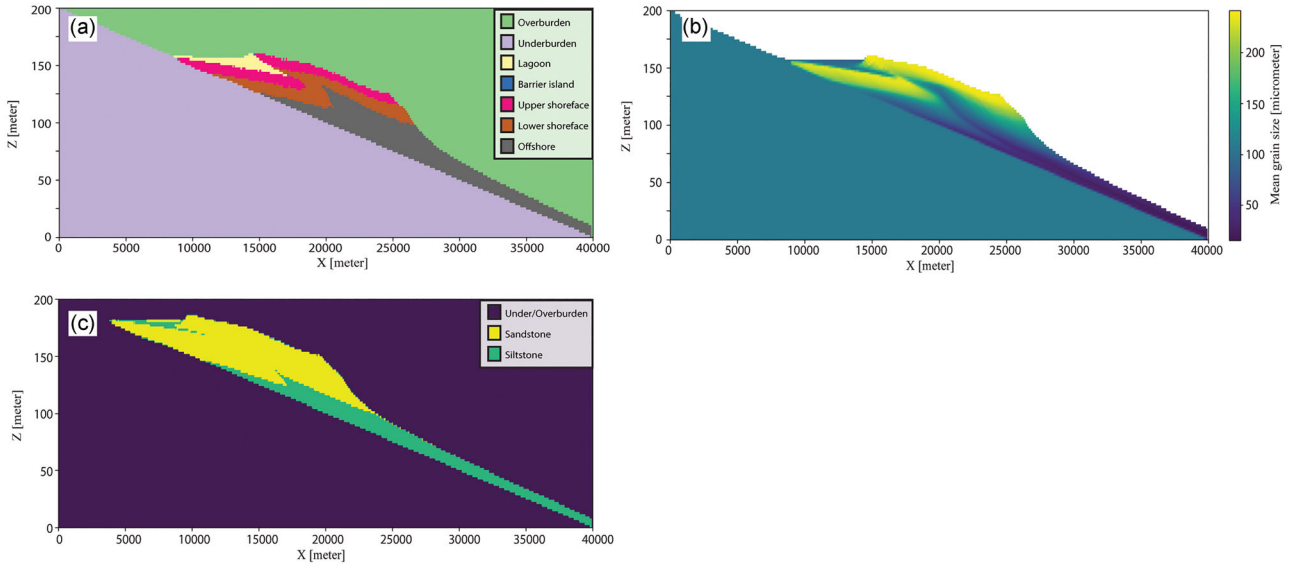


**FIGURE 3** Reference geological simulation generated by pyBarSim. Input parameters can be found in Supporting Material 1. The output files include the facies distribution (a), mean grain size (b) and lithology distribution (c). Lithology is assigned applying the conditions described in Step 1: Generation of geological simulations using stratigraphic modelling tools section. Z indicates the thickness of the simulated reservoir model and X, the lateral extension. Here, only a part of the overburden is included to better appreciate the small-scale, stratigraphic heterogeneities.

on depositional environment: lagoon, barrier island, upper shoreface, lower shoreface and offshore. The outputs related to the grain size distribution include the ratio per cell of each grain size class and the mean grain size (Figure 3b). For this simulation, there are four grain size classes. The finest, simulated grain size class is 5 μm, corresponding to fine silt. The coarsest grain size class is 250 μm, corresponding to the limit between medium and fine sand. Thus, the lithology distribution includes three labels (Figure 3c): sandstone, siltstone and underburden and overburden together.

These three outputs—grain size, facies and lithology—are used to create different distributions of mass-density and P-wave velocity at different levels of discretization. The most detailed labels are those of grain size–based simulation, with unique values for every cell of $2 \times 2$ m$^2$. A more discretized property distribution is based on the facies distribution, with five labels within the simulation. The greatest level of discretization is achieved when using the lithology for the distribution of petrophysical and acoustic properties, with two labels within the simulation. The acoustic property distribution method is described in Step 2: Population of acoustic property values section. Table 1 includes the average values of mass-density and P-wave velocity calculated for each lithology and facies label. The resulting P-wave velocity and mass-density distributions are displayed in Figure 4.

The properties of the overburden and underburden are the same for the three simulations.

Due to computational limitations, the reference simulation of over 40 km on the horizontal dimension had to be divided into sections. Seven sections of 7600 m and a smaller eight section were created. To ensure the full imaging of all the areas on the simulation, there is an overlap of 1800 m between sections. Supporting Material 2 includes more details on the start and end locations for each section.

**TABLE 1** Average values of mass-density (kg/m$^3$) and P-wave velocity (m/s) calculated based on the grain size–based simulation for all the categories within the lithology and facies simulations.

| Label | Mass-density (kg/m$^3$) | P-wave velocity (m/s) |
|---|---|---|
| **Lithology** | | |
| Sandstone | 2078 | 3149 |
| Siltstone | 2226 | 2937 |
| **Facies** | | |
| Lagoon | 2225 | 3199 |
| Barrier island | 2035 | 3123 |
| Upper shoreface | 2047 | 3146 |
| Lower shoreface | 2084 | 3164 |
| Offshore | 2205 | 2984 |

*Note*: All grid cells of the grain size–based simulation have a lithology and a facies label. By considering all the cells with the same label, the average mass-density and P-wave velocity values are calculated.

## Input parameters for forward seismic modelling and migration

Once the P-wave velocity and mass-density simulations are obtained, the time-domain finite difference method, based on first-order acoustic wave equations, as explained in Step 3: Forward seismic modelling and migration section, is used for

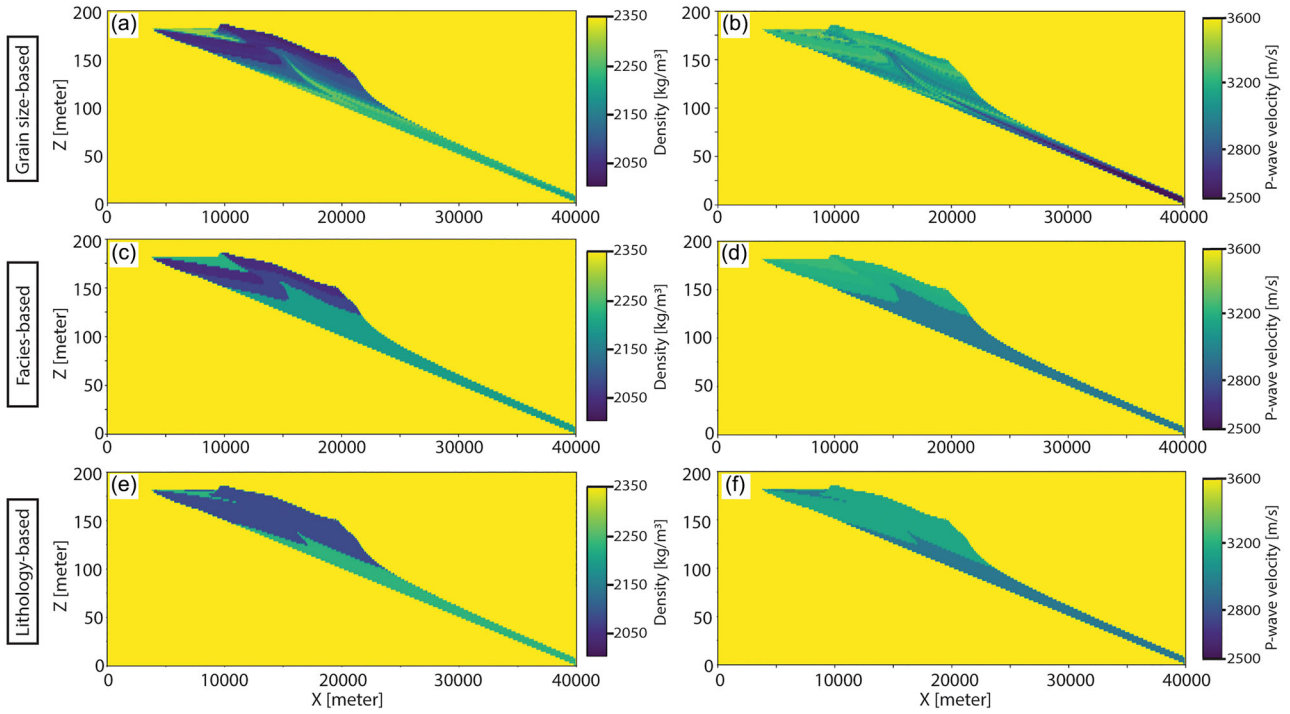


**FIGURE 4** Mass-density (kg/m$^3$) and P-wave velocity (m/s) distributions for the simulations: grain size distribution-based, method (a—mass-density; b—P-wave velocity), facies-based discretized (c—mass-density; d—P-wave velocity), and lithology-based discretized (e—mass-density; f—P-wave velocity). Note that the same colour scale has been used for all the subfigures of the same property. Z indicates the thickness of the simulation and X, the lateral extension, both in meters. Note that only part of the overburden is included in the figure.

forward modelling, including the target area and the 1100-m-thick overburden. The source wavelet is a Ricker source. For the data acquisition plan, we employ a fixed spread scheme: All receivers are positioned at the surface, covering the entire range of the model at intervals of 2 m. All sources are also positioned at the surface, covering the entire range of the model at intervals of 10 m. The time sampling rate is 0.002 ms, and the recording length is 1.2 s. For the full-wavefield migration–angle dependent, the source sampling and the receiver sampling are chosen as 10 and 2 m, respectively. The frequency range is compatible with the modelling frequency range of 5–150 Hz. A smooth velocity model and the maximum and minimum velocity ranges are also derived from the forward modelling velocity models to be used in the migration step. Considering the average model's velocity and the maximum frequency used for the seismic modelling, it is our observation that the minimum layer thickness that can be distinguished in the reservoir model is 14 m.

## RESULTS AND INTERPRETATION

### P-velocity and density contrast

This section explores the difference in properties among the three simulations. On average, the mass-density values are 8% higher for the grain size–based distribution when compared to the facies-based discretization, with the differences varying between −5% and +10%. There is a greater range of variation for P-wave velocity. The mean difference in P-wave values is 3%, with higher values for the facies-based simulation. The range goes from +23% to −15%. Within the facies-based simulation, some of the labels show very similar velocity and density values (Table 1).

When considering the difference in mass-density values between the grain size-based distribution and the lithology-based discretization, the mean difference is 1%, with higher values when using lithology-based discretization. This difference varies between −9% and +9%. On average, the P-wave velocity values are 6% lower for the discretized model, with a range of difference that goes from −13% to +23%.

With the information about the variation of mass-density and P-wave velocity, we can calculate the expected variations in the impedance. Taking into account the average percentage difference in the case of lithology-based discretization, the impedance variation is 11%, and for the facies-based discretization, it is 7%. However, if we consider the maximum variations observed in the acoustic properties, we can expect changes in impedance of 35% for the lithology-based and 34% for the facies-based. In both cases, the resulting reflection coefficient is around 0.15.

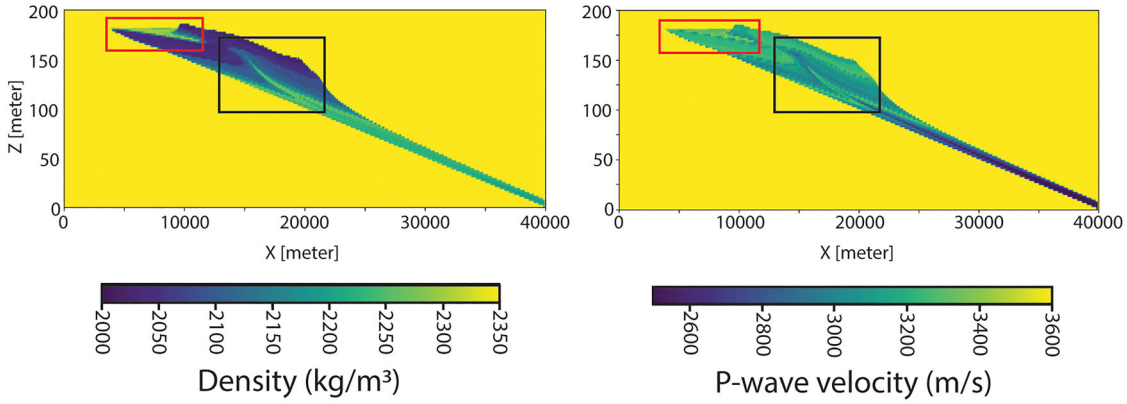


**FIGURE 5** Acoustic property distribution for the grain size–based simulation showing the two areas where the main differences among discretization levels are observed. The red square highlights location one and the black square, location two. More detailed images and analysis of the differences between discretized levels in Figures 6 and 7 and Location 1. and Location 2 sections. Note that only part of the overburden is included in the figure.

## Mapping the differences in seismic response

This study focuses on the most relevant differences of the seismic data among the three discretization levels. Those differences are concentrated in two locations (Figure 5). The first location is associated with a high-density and high-velocity area that develops at the top left of the geologic simulation (Figure 5, red square). This location is partially related to the lagoon facies, and it is composed of sandstone and siltstone (Figure 3). The second location is a stratigraphic structure composed of high-density and high-velocity sediments that results from the increase in relative sea level (Figure 5, black square). This location is composed of sediments from the offshore, lower shoreface and upper shoreface facies, and it is composed of sandstone and siltstone (Figure 3).

The Supporting Information section includes a comparison among the different levels of discretization for all the sections. These images include P-wave velocity distribution, mass-density distribution and seismic reflection figures, with indications on the main differences in zoomed seismic images. Section number 7 of the simulation is not included because of the lack of resolution to distinguish the impact on the seismic response of small-scale heterogeneities. With the current input parameters, in those areas where the target is thinner than 14 m, only the reflectors related to the top and the bottom of the target are observed. This thickness threshold is reached in Conclusion.

### Location 1

The first major contrast on seismic response is located on the upper left side of the simulation (Figure 5, red square). On the blowup image, we observe a high-density and high-velocity area for the grain size–based simulation (Figure 6a). For the facies-based simulation, the density contrast is still high, but the velocity distribution shows smooth transitions between facies. For the lithology-based simulation, there is an alternation of lower and higher density/velocity areas. These differences in the distribution of acoustic properties translate into two major distinctions on the seismic response, here labelled zone A and zone B (Figure 6b).

Zone A marks the contact between the high-density, high-velocity area and an area with lower density and velocity values (Figure 6a). It is also related to a shift of facies and a change of lithology. But the main changes in properties occur with different property contrasts and at slightly different locations around zone A (Figure 6a). The particular geometry of each change affects the continuity, thickness and amplitude values of Reflector 1 (Figure 6b). This area develops due to the contrasting sedimentological characteristics of the lagoon (greater ratio of fine sediment) and the upper shoreface (greater ratio of coarser sediment) (Figure 3). As a result of the implemented methodology for the allocation of acoustic properties, areas with a greater proportion of fine sediments lose more porosity during compaction than areas dominated by coarser sediments, which results in higher mass-density values (Figure 6a).

Because the contrasting properties are associated with changes in facies, we find more similarities between the seismic response of the grain size–based and facies-based simulations (Figure 6b). The lithology-based simulation does not capture these changes adequately. We also observe that the contact between upper shoreface and lagoon does not fit with the main changes in mass-density and P-wave velocity variations, which actually occur within the lagoon facies, resulting in different thicknesses of Reflector 1 (Figure 6b).

Zone B marks the variation of acoustic property values in the vertical direction throughout the simulations (Figure 6a). The location and the intensity of the changes in density and velocity vary from one level of discretization to another. This translates into different thickness and amplitude values

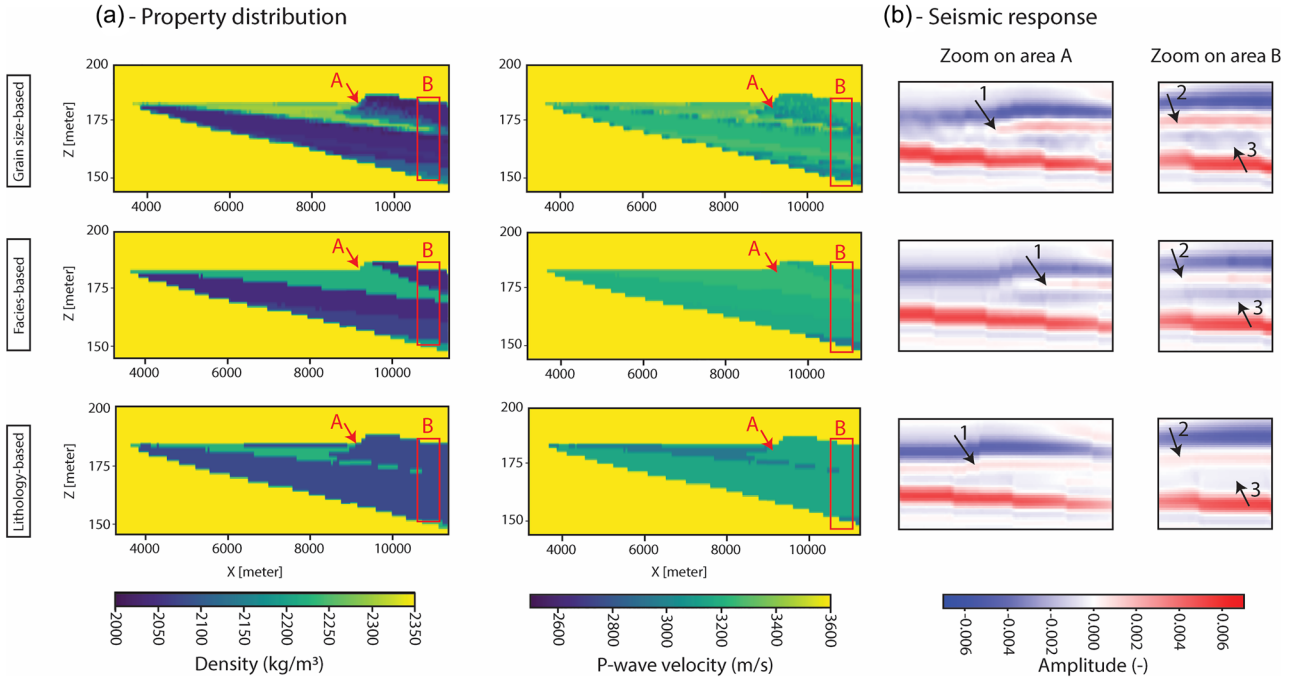


**FIGURE 6** (a) Blowup of the location one indicated in Figure 5 with the density (kg/m$^3$) and P-wave velocity (m/s) distributions for each discretization level. A and B indicate the areas where the seismic response differences are observed. (b) Blowup of the seismic response (in amplitude, unitless) of areas A and B. The main differences have been indicated with numbers from 1 to 3 to aid the comparison between simulations.

of Reflector 2 and the amplitude distribution of Reflector 3 (Figure 6b). The behaviour in amplitude values of Reflector 3 is of special interest. This reflector is characterized by a very low and constant amplitude value for the whole highlighted region in the lithology-based simulation, which matches with the mass-density and P-wave velocity distributions, where the only difference is related to local cells labelled silt, responsible for the transition from Reflectors 2 to 3 (Figure 6b). Reflector 3 is also represented by a smooth distribution of amplitude values for the facies-based simulation, with lower values towards the contact with the lowermost reflector that represents the base of the target. This smooth distribution is related to the smooth changes in P-wave velocity and mass-density that result from applying a single, averaged value per facies (Figures 4 and 6). However, in the grain size–based simulation, the amplitude value distribution is more spotty, which relates to local changes in grain size distributions and the consequent local changes in P-wave velocity and mass-density (Figure 6). It is also observable that the distribution of properties within the upper and lower shoreface facies is almost as constant as in the facies-based simulation (Figures 3, 4 and 6).

## Location 2

A second significant contrast in the seismic response is located in the central part of the simulations (Figure 5, black square). A high-density and high-velocity area for the grain size–based simulation is located in the middle, surrounded by lower density and velocity values, that merges with a second high-density and high-velocity layer at the bottom of the simulation (Figure 7a). For the facies-based discretization, both the density and velocity contrasts are high between the offshore and lower shoreface facies. For the lithology-based discretization, there is a contrast between siltstone and sandstone in density/velocity. These contrasts of acoustic properties are reflected in the seismic response of three zones (Figure 7b, labelled zones C–E), which spread throughout almost the whole simulation. The architecture observed in the distribution of properties is related to a relative sea level rise, which forces a migration of the facies and, in general, the deposition of coarser sediments towards the land and a following, progressive, relative sea level fall.

Zone C is characterized by a higher density and lower velocity layer on the grain size–based simulation (Figure 7a). This layer is not registered in the lithology-based discretization, because the changes in grain size distributions do not imply a change in lithology (Figure 3). On the facies-based discretization, the facies show a trend that matches with the orientation of the layer but with lower contrasts (Figure 7), which results from allocating averaged values of mass-density and P-wave velocity. These distinctions can also be observed on the seismic data with changes in continuity, thickness and amplitude intensity on Reflectors 4 and 5 (Figure 7b). The general geometry of the layer that we observe in the grain size–based simulation is also observable on the seismic

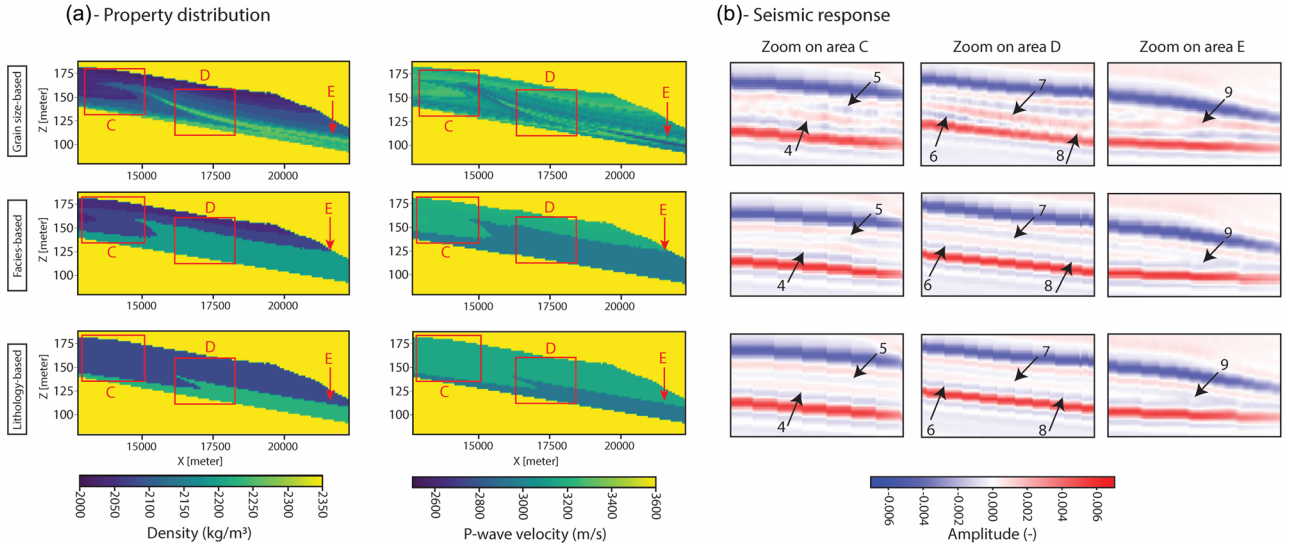


**FIGURE 7** (a) Blowup of the location two indicated in Figure 5 with the density (kg/m$^3$) and P-wave velocity (m/s) distributions for each discretization level. C, D and E indicate the areas where the seismic response differences are observed. (b) Blowup of the seismic response (in amplitude, unitless) of areas C, D and E. The main differences have been indicated with numbers from 4 to 9 to aid the comparison between simulations.

response of the facies-based simulation, where Reflector 5 has a notable lateral change of the amplitude value (Figure 7b), but the lateral extension of the structure is not fully captured.

Zone D is characterized by two features: (1) a progressive mass-density and P-wave velocity change in the vertical direction on the grain size-based simulation; (2) the merging of the high velocity and density layer that crosses the simulation with another high velocity and density layer at the bottom of the target (Figure 7a). This structure is only registered as one facies change for the facies-based simulation and one lithology alternation for the lithology-based simulation (Figure 7a). The seismic response for the facies- and lithology-based simulations is a parallel alternation of reflectors, with a slight change in the thickness and amplitude intensity, especially of Reflector 7 (Figure 7b). When comparing to the grain size–based simulation, it is observed that the blue reflector (6 and 8), which was continuous for the other simulations, is here discontinuous and showing significant thickness variations. The seismic response is dominated by the shape and distribution of Reflector 7, which represents the high density and velocity layer mentioned above. Reflector 7 also controls the thickness and continuity of the blue reflectors above and below.

Zone E shows the lateral thinning of the target and the internal heterogeneity (Figure 7a). For the lithology- and facies-based simulations, there is only one change in lithology and one in facies, respectively. The complexity is higher for the grain size–based simulation, with the appearance of a low velocity/density area in between the high velocity and density layers mentioned in the previous paragraph (Figure 7a). This contrast has an impact on the continuity and geometry of Reflector 9 versus the blue reflector (Figure 7b). The strong contrast in P-wave velocity and density registered at the bottom of the grain size–based simulation enhances the lateral continuity of the blue reflector and the merging of the two red reflectors. This observation opposes the geometry of the reflectors in the lithology- and facies-based simulations.

## DISCUSSION

### Gibbs' phenomenon: Why are there reflectors where there is no property contrast?

When spatial discontinuities occur, they require infinite frequency content to be fully characterized. But in practice, seismic measurements have a finite bandwidth, partly by the acquisition devices, but mostly due to absorption in the Earth during wave propagation (Yilmaz, 2001; Aki & Richards, 2002). This limitation will cause ringing artefacts in the imaged reflectivities, leading to unwanted echoes in or edge distortion in our images (Chhoa, 2020). The phenomenon responsible for these unwanted echoes is known as the Gibbs' phenomenon and occurs when in seismic images when a band-limited signal is reflected at a sharp contrasts, resulting in high-frequency oscillations and inaccuracies near the discontinuities.

As depicted in Figure 8, there are some changes in the seismic amplitude (Figure 8g–i, black arrows) that are not linked to changes in mass-density or P-wave velocity (Figure 8a–f). These ringing effects will interfere with the reflections that are related to acoustic property changes (Figure 8a,b, and related, red arrows). Because of this interference, the change

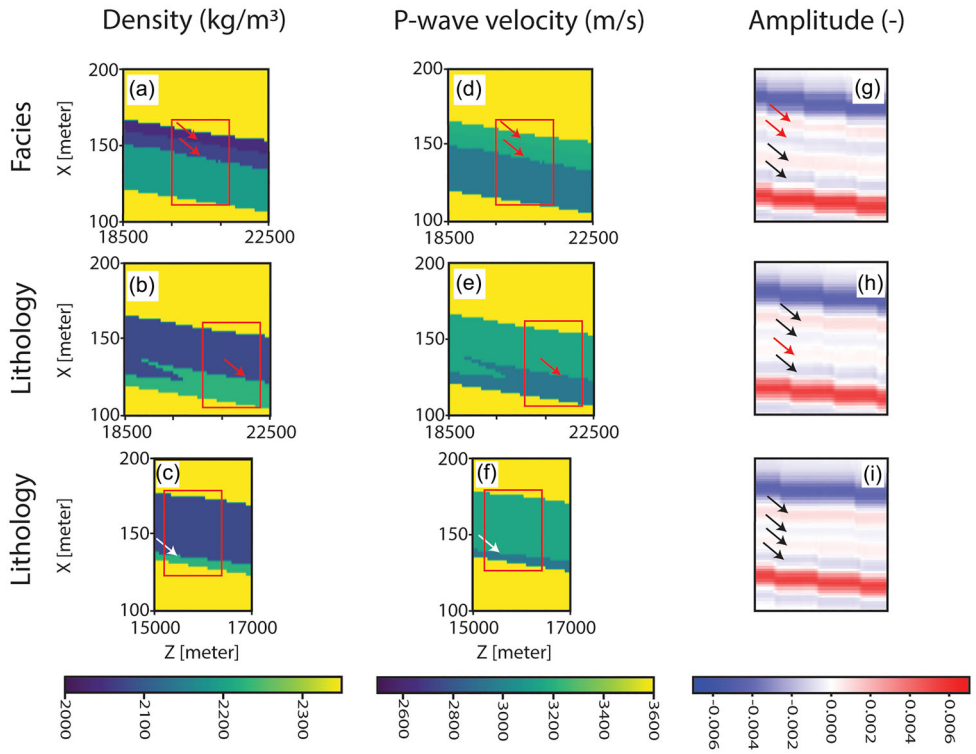


**FIGURE 8** Examples of locations in our models with only one (b, c, e and f) or two (a and d) changes in acoustic properties but where four reflectors (g–i) are generated in the synthetic seismic data (black arrows). The density (kg/m$^3$), P-wave velocity (m/s) and a blowup of the amplitude values of the seismic data (unitless) are included. Arrows in red indicate the changes in density and P-wave velocity (a, b, d, and e) and where they can be observed in the seismic response (g and h). In the lowermost example, the change cannot be observed because the thickness of the layer is below the resolution threshold (white arrows) (c, f and i). The generation of these reflectors is linked to the Gibbs' phenomenon (g, h and i).

in reflection coefficients is not the sole factor influencing the generation of patterns in reflectivity images. This can pose challenges for interpretation by giving the false impression about the existence of sublayers with contrasting acoustic properties. We only observed this phenomenon in our facies- and lithology-based simulations.

There are several methods available to mitigate these artefacts to some extent, by imposing extra constraints or weights during the imaging process, but none of them were applied in our workflow (Abolhassani & Verschuur, 2024; Chhoa, 2020).

## Impact of discretization on the small-scale, stratigraphic heterogeneities

The data depicted in Figures 6 and 7, together with the material in Supporting Material 3, show that the level of discretization has an impact on the seismic response. Creating simulations that are based on stratigraphic modelling and where the acoustic properties are assigned based on grain size distributions preserves the representation of small-scale, stratigraphic heterogeneities within specific facies or lithologies (Figures 6 and 7). Table 2 includes a compilation of the described zones and the specific improvements in the imaging for this specific case of wave-dominated, shoreface systems. The observed structures sometimes develop in different depositional environments and are composed of different lithologies (Figures 5–7). When allocating a single value to one facies/lithology, these structures are no longer represented, and, therefore, it is not possible to recognize them in the seismic response.

Being able to distinguish small-scale, stratigraphic heterogeneities with strong velocity and/or density contrast and isolate their location from the surrounding sediments will help understand how the fluid flow might behave inside the reservoir. In our method, the calculation of mass-density and P-wave velocity is strongly dependent on the porosity. This means that high velocity and density layers are also characterized by lower porosity values. In grain size classes varying from silt to medium sand, lower porosity values tend to relate to lower permeability (Chilingar, 1964). The opposite occurs with layers with high porosity values. For subsurface locations where the relationship between porosity and permeability is well understood, this method can help identify areas with higher or lower permeability values, which will behave as pathways or barriers for the fluid flow. Our method has shown that the use of stratigraphic modelling can capture the

**TABLE 2** Summary of the improvements in the seismic imaging that have been observed for each zone when applying the grain size–based distribution of acoustic properties. For each zone, we include the lithologies and facies involved, and a short description of the structures that are better images.

| Zone | Lithology | Facies | Improvement |
|---|---|---|---|
| A | Sandstone and siltstone | Lagoon | – Accurate imaging of the contact between the high density/velocity and the low density/velocity area within the lagoon<br>– Better definition of the lateral extend of the low density/velocity layer related to upper shoreface deposits |
| B | Sandstone | Lagoon, upper and lower shoreface | – Better definition of the thickness of the upper shoreface section on top of the lagoon<br>– Detailed imaging of the density/velocity changes within the upper and lower shoreface |
| C | Sandstone | Upper and lower shoreface, offshore | – Detailed definition of the structure and density/velocity variations resulting from the relative sea level rise |
| D | Sandstone and siltstone | Lower shoreface, offshore | – Detailed imaging of the structure and density/velocity variations resulting from the relative sea level rise |
| E | Sandstone and siltstone | Lower shoreface, offshore | – Better definition of layer pinch-out towards offshore deposition |

presence of these heterogeneities, and they can be recognized in synthetic seismic data.

In this paper, the acoustic property values from the grain size–based simulation were used to calculate the corresponding values for the facies- and lithology-based simulations. The values were calculated by averaging all the cells with the same lithology or facies label, as explained in the Reference geological simulation section. This method of averaging, but with core data, has also been used in other forward seismic modelling papers (Grippa et al., 2019). In other cases, they have referred to typical velocity and density values for stratigraphic units in particular sedimentary basins (Falivene et al., 2010; Anell et al., 2016), which we assumed to be averaged values as well. In the case of the facies-based simulation, applying averaging techniques for the calculation of properties smoothens the internal contrast within the facies and results in similar values for acoustic properties for different facies, except for the offshore and the mass-density of the lagoon (Table 1). Therefore, the transition among some of the facies is not clearly observed in the seismic data (Figure 6, area B).

When comparing the different discretization levels, some resemblance between the seismic responses of the three simulations is observed. First, the geometry of the seismic response of the facies-based and grain size–based simulations are similar for areas A and C described in the Mapping the differences in seismic response section (Figures 6 and 7). However, there is strong contrast in the amplitude variations and, particularly for area A, in the lateral extension of the reflectors (Figure 6). Second, the seismic response of the lithology- and the facies-based simulations for areas D and E are similar (Figure 7). These seismic responses are characterized by a rhythmical alternation of reflectors for area D, and the merging of two blue reflectors in area E (Figure 7). However, the seismic response of the grain size–based and lithology-based simulations does not show resemblance for any of the highlighted cases. Consequently, for the case of wave-dominated shoreface systems, the use of lithology-based simulations when analysing small-scale, stratigraphic heterogeneities will result in the least precise characterization of the subsurface target.

## Implications on seismic inversion and geological modelling

In this paper, we have shown that the way we discretize the acoustic properties of the subsurface has an impact on the seismic response, and that, if we allocate properties based on lithology or facies classifications, some small-scale, stratigraphic heterogeneities will be erased from our seismic data. These findings have an impact on the way inversion of seismic data is traditionally performed. Seismic inversion aims at transforming seismic data from the subsurface into elastic properties, which can then be used in petrophysical and geological modelling to build 3D models of other valuable properties for reservoir characterization (Ostrander, 1984; Shuey, 1985; Neidell, 1986; Sheriff & Geldart, 1995). A key challenge is to quantify the uncertainty due in part to the lack of resolution of seismic data, which blurs small-scale heterogeneities.

Owing to their unique mathematical properties, (multivariate) Gaussian distributions have become a cornerstone of inversion workflows to capture uncertainties in the spatial variations of subsurface properties (Jullum & Kolbjørnsen, 2016; Grana, 2018; Pendrel & Schouten, 2020). But the results of this study show that the application of Gaussian

distributions is not able to resolve the architectural features observed in the geological simulations.

In the case of properties such as porosity, the available data to condition the posterior distribution are based on well log and core data. From those data, an autocovariance or a semivariogram model is traditionally used to capture the spatial variability of those properties in the subsurface. But variations of sea level and sediment supply lead to elongated, curved and non-stationary structures, the properties of which are discontinuous along erosional surfaces, all features that cannot be represented based on a single-covariance model (Journel, 2005).

However, our results highlight that small-scale, stratigraphic heterogeneities that develop at scales below lithology or facies have an impact on the seismic response. So modelling properties as constant values for each facies or lithology—as is sometimes done to simplify geological modelling based on lithofacies, lithotypes or litho/fluid distributions (Merletti & Torres-Verdín, 2006; Cardiff & Kitanidis, 2009; Roncarolo & Grana, 2010; Kemper & Gunning, 2014; Mur & Waters, 2018; Grana, 2019)—leads to ignoring valuable information available in the data. At the same time, the resolution of seismic data is rarely high enough to unambiguously characterize those heterogeneities. In that context, a covariance model is too weak as a geological prior to compensate for the lack of data. This raises the question of the true predictive power of the models obtained through inversion based on multivairate Gaussian distributions.

In recent years, researchers have tried to overcome the limitations of the Gaussian assumption by developing other approaches for the definition of the prior and posterior distributions (Grana, 2018, and references herein). Elongation, curvature and, more generally, non-stationarity can be captured in Gaussian simulations but only using advanced approaches with a higher modelling cost (Boisvert et al., 2009; Machuca-Mory & Deutsch, 2013; Fouedjio, 2017). Multiple-point approaches provide a more straightforward solution to use more geologically plausible priors (Liu et al., 2004; González et al., 2008; Cordua et al., 2012), although the geological structures are rarely perfectly preserved.

We consider that the current approach of seismic inversion workflows should be reconsidered to better capture small-scale, stratigraphic heterogeneities. Some studies that include geological conditioning in the inversion process have shown its impact on the quantitative risking of reservoir's prospectivity, especially in areas with limited well information (Gonzalez et al., 2016; Crepaldi et al., 2024), and on $CO_2$ monitoring (Barajas-Olalde et al., 2021). Here, we suggest adding the use of forward stratigraphic modelling (FSM) to the workflow for seismic data inversion. This way we can account for the changes in properties and the resulting small-scale, stratigraphic heterogeneities that occur below facies or lithology scale. For this, it is necessary to develop fast and flexible stratigraphic modelling tools and procedures to generate acoustic properties that fit the targets in the subsurface.

This paper focuses on wave-dominated, shoreface environments and stratigraphic heterogeneities that develop in such depositional environments. Future work can apply the same method to other depositional environments. To do so, it is necessary to evaluate the available FSM tools for other depositional environments and their compatibility with the method used for this study. There are stratigraphic modelling tools for deep-water channels (Pyrcz et al., 2012), fluvial systems (Willis & Tang, 2010) and tide- and/or fluvial-dominated shallow marine environments (SedSim, Tetzlaff & Harbaugh, 1989; Tetzlaff, 2005).

## Methodology limitations

The method used to create the grain size–based simulations has a series of limitations. First, the selection of the stratigraphic modelling tool is limited to those that are able to generate small-scale stratigraphic heterogeneities at meter scale and that provide grain size distribution data as output, typically in the form of the proportion of different grain size classes. There are different types of stratigraphic modelling tools, and within rule-based tools, two of the main drawbacks are the limitation for log data conditioning and the limitation to simulate different depositional environments in the same tool (Pyrcz et al., 2015). In this regard, rule-based modelling tools approximate the physical processes that control erosion and deposition to a series of rules, rules that are specific for each depositional environment and that represent processes that are active in each environment. Further effort is required to develop more robust tools that can handle different rulings for different depositional environments within the same simulation (Pyrcz et al., 2015). There are also process-based modelling tools where the resulting property distributions are based on physical laws that control the erosion, transport and deposition of sediment (Pyrcz et al., 2015). However, this type of tool tends to resolve diffusion equations that approximate the real processes active in nature to be able to handle modelling through large areas for long modelling times (from thousands to millions of years) (Tetzlaff & Harbaugh, 1989; Harbaugh, 1993; Granjeon & Joseph, 1999).

Second, for the calculation of the acoustic properties, a number of assumptions are made. In the proposed method, allocation of initial porosity depends on the experimental values obtained by Beard and Weyl (1973), who used fluvial sand samples to relate initial porosity, mean grain size, and sorting. Those measurements did not account for variations in roundness and sphericity of the grains. However, roundness and sphericity change from one depositional environment to another (Patro & Sahu, 1974). Roundness and

sphericity impact the packing of the grains and, in consequence, the porosity (Beard & Weyl, 1973; Cho et al., 2006; Suh et al., 2017). Thus, we cannot confirm that, for the same mean grain size and sorting relationships, we would obtain the same initial porosity values in a wave-dominated coastal environment.

In our method, we have calculated the final porosity by implementing a porosity loss constant (Wendebourg & Harbaugh, 1997). This is necessary because pyBarSim simulates sedimentation at surface conditions, but rocks in the subsurface experience compaction and, in many cases, diagenetic processes that change the arrangement of grains and the porosity (Bjørlykke & Høeg, 1997). Porosity loss curves are lithology and basin dependent (Allen & Allen, 1990), and there are other equations that can be used to calculate the final porosity (Hubbert & Rubey, 1959; Sclater & Christie, 1980; Baldwin & Butler, 1985; Allen & Allen, 1990; Giles, 1997). Diagenetic processes, such as cementation, might also affect specific facies or areas above others, creating velocity and density contrast that might not be related to grain size variations alone.

For the calculation of mass-density, values for the density of the grains and the density of the fluid filling the pore space are required. We assumed that the sediment is only composed by quartz particles, a simplification of the sediment composition in siliciclastic systems, and that the porosity is water saturated. However, the sediment composition of wave-dominated shoreface systems can vary from mainly quartz to calcite-dominated, with many other accessory minerals and possible combinations. These parameters can be modified to better fit sediment and fluid compositions observed in subsurface data and analyse the impact of these changes on the seismic response.

For the calculation of P-wave velocity, we use an empirical equation that relates porosity, clay content and effective pressure (Eberhart-Phillips et al., 1989). Here, the finest grain size class used as input for BarSim has a diameter of 5 μm and is classified as fine silt (Folk, 1954). Therefore, we assumed that the clay content equals the proportion of fine silt. We have also assumed the effective pressure to be equivalent to 1000 m depth. There are other empirical equations that explore the relationship between clay content and porosity (Han et al., 1986), but they do not take effective pressure into account, and so they were discarded. It is also worth noting that the empirical equations are based on lab sample measurements and that no upscaling methods have been applied to the acoustic properties. Research has shown that the impact of the properties controlling the wave velocities at laboratory scale might decrease in presence of other structural features (Bailly et al., 2019).

There are also some limitations in the numerical seismic modelling and migration process that have an impact in the vertical resolution of the synthetic seismic data. The vertical resolution depends on the frequency content of the seismic waves and the subsurface velocity model (Cox et al., 2020). Assuming a maximum frequency of 150 Hz and an average P-wave velocity of 3600 m/s in the target area, the detection resolution, which is normally approximated to 1/4 of the wavelength, is 6 m, and the resolution to distinguish the presence of stratigraphic features, which is approximated to 1/10 of the wavelength, is around 2.5 m (Yilmaz, 2001).

Also note that by limiting ourselves to 2D and acoustic modelling, we have still made simplifications of the reality, which is a 3D elastic Earth. However, it is our belief and expectation that the conclusions we made on the discretization of the geologic models and the link to seismic resolution will not change by making all modelling more realistic. But strictly speaking, this has to be proven still in follow-up research.

On a final note, this research still uses a discretized distribution of properties, a discretization based on a continuous property. Lithology and facies are labels used to simplify the complexity of the subsurface, where the heterogeneities are the result of the change in continuous properties, such as grain size. In our simulations, the $2 \times 2$ cells result from the interpolation of grain size changes within that area, and it is already able to add more detail to the simulations. The finer our grid is, the better we could capture the real distribution of the properties in subsurface. However, we have shown that avoiding the discretization based on lithology or facies already brings improvement to the imaging of the stratigraphic architecture of the target area. In addition, this seems to be the right path to fine-tune seismic inversion methodologies applied to real seismic data.

## CONCLUSION

This paper shows that simulated meter-scale, stratigraphic heterogeneities of grain size distributions have an impact on the synthetic seismic response. To analyse these heterogeneities, we introduce a method that links the generation of geological simulations using stratigraphic modelling and the allocation of acoustic properties based on grain size distribution. Even with its limitations, this method enables improved observations of stratigraphic heterogeneities in the seismic response versus the simulations with discretized acoustic properties. The imprint of these heterogeneities is modified or disappears when we classify the detailed grain size distribution data into facies and, especially, into lithology, as this results in a single, averaged values of acoustic properties per facies and/or lithology class.

Our results also highlight the limitations of the conventional, lithology-based seismic inversion workflows and Gaussian-based uncertainty analysis. We have proven that discretizing simplifies the complexity contained within certain facies or lithologies and fails to capture the impact of

gradual changes of density and P-wave velocity that are related to gradual porosity and grain size distribution changes. The grain size–based simulation better captures the curved architecture and property changes that result from relative sea level variations.

For the case of clastic, wave-dominated shoreface environments and under the input parameters that we set, we have observed the impact of discretizing mass-density and P-wave velocity in three situations: (1) the property changes within the sediments that constitute the lagoon area; (2) the architecture and property contrast between lower shoreface, upper shoreface and offshore after a relative sea level rise and the subsequent sediment deposition during sea level fall; (3) the architecture and property distribution in the lower shoreface to offshore transition and the reservoir thinning.

## ACKNOWLEDGEMENTS

The Delphi Consortium (delphi-consortium.com) is the funder ofthis research. The authors thank the continued support of the sponsors of this consortium.

## DATA AVAILABILITY STATEMENT

The data that support the findings of this study are confidential under the Delphi Consortium Agreement. However, upon reasonable request, we can ask permission for sharing (part of) the data. Part of the method is based on an open-source package, pyBarSim, which is available at https://github.com/grongier/pybarsim.

## ORCID

*Andrea Cuesta Cano* https://orcid.org/0000-0002-7017-6031
*Joep Elisabeth Anton Storms* https://orcid.org/0000-0002-8902-8493
*Guillaume Rongier* https://orcid.org/0000-0002-5910-6868
*Allard Willem Martinius* https://orcid.org/0000-0002-6414-6274

## REFERENCES

Abolhassani, S. & Verschuur, D.J. (2024) Efficient preconditioned least-squares wave-equation migration. *Geophysics*, 89(3), S275–S288. Available from: https://doi.org/10.1190/geo2023-0048.1

Aki, K., & Paul, G. R. (2002). Quantitative Seismology. Vol. 2. CA: Univ. Sci. Books. Sausalito. 700.

Allen, P.A. & Allen, J.R. (1990) *Basin analysis: Principles and applications*. Oxford: Blackwell Scientific Publications.

Anell, I., Lecomte, I., Braathen, A. & Buckley, S.J. (2016) Synthetic seismic illumination of small-scale growth faults, paralic deposits and low-angle clinoforms: a case study of the Triassic successions on Edgeøya, NW Barents Shelf. *Marine and Petroleum Geology*, 77, 625–639. Available from: https://doi.org/10.1016/j.marpetgeo.2016.07.005

Anthony, E.J. (2013) Storms, shoreface morphodynamics, sand supply, and the accretion and erosion of coastal dune barriers in the southern North Sea. *Geomorphology (Amsterdam, Netherlands)*, 199, 8–21. Available from: https://doi.org/10.1016/J.GEOMORPH.2012.06.007

Anthony, E.J. & Aagaard, T. (2020) The lower shoreface: morphodynamics and sediment connectivity with the upper shoreface and beach. *Earth-Science Reviews*, 210, 103334. Available from: https://doi.org/10.1016/J.EARSCIREV.2020.103334

Armitage, D.A. & Stright, L. (2010) Modeling and interpreting the seismic-reflection expression of sandstone in an ancient mass-transport deposit dominated deep-water slope environment. *Marine and Petroleum Geology*, 27(1), 1–12. Available from: https://doi.org/10.1016/J.MARPETGEO.2009.08.013

Backstrom, J., Jackson, D., Cooper, A. & Loureiro, C. (2015) Contrasting geomorphological storm response from two adjacent shorefaces. *Earth Surface Processes and Landforms*, 40(15), 2112–2120. Available from: https://doi.org/10.1002/ESP.3788

Bailly, C., Fortin, J., Adelinet, M. & Hamon, Y. (2019) Upscaling of elastic properties in carbonates: a modeling approach based on a multiscale geophysical data set. *Journal of Geophysical Research: Solid Earth*, 124(12), 13021–13038. Available from: https://doi.org/10.1029/2019JB018391

Bakke, K., Gjelberg, J. & Agerlin Petersen, S. (2008) Compound seismic modelling of the Ainsa II turbidite system, Spain: application to deep-water channel systems offshore Angola. *Marine and Petroleum Geology*, 25(10), 1058–1073. Available from: https://doi.org/10.1016/j.marpetgeo.2007.10.009

Bakke, K., Kane, I.A., Martinsen, O.J., Petersen, S.A., Johansen, T.A., Hustoft, S. et al. (2013) Seismic modeling in the analysis of deep-water sandstone termination styles. *AAPG Bulletin*, 97(9), 1395–1419. Available from: https://doi.org/10.1306/03041312069

Baldwin, B. & Butler, C.O. (1985) Compaction curves. *AAPG Bulletin*, 69(4), 622–626.

Barajas-Olalde, C., Mur, A., Adams, D.C., Jin, L., He, J., Hamling, J.A. et al. (2021) Joint impedance and facies inversion of time-lapse seismic data for improving monitoring of $CO_2$ incidentally stored from $CO_2$ EOR. *International Journal of Greenhouse Gas Control*, 112, 103501. Available from: https://doi.org/10.1016/j.ijggc.2021.103501

Beard, D.C. & Weyl, P.K. (1973) Influence of texture on porosity and permeability of unconsolidated sand. *AAPG Bulletin*, 57(2), 349–369. Available from: https://doi.org/10.1306/819A4272-16C5-11D7-8645000102C1865D

Berkhout, A.J. (Guus). (2014) Review paper: an outlook on the future of seismic imaging, Part I: forward and reverse modelling. *Geophysical Prospecting*, 62(5), 911–930. Available from: https://doi.org/10.1111/1365-2478.12161

Bhattacharya, J. & Walker, R.G. (1991) River- and wave-dominated depositional systems of the upper cretaceous dunvegan formation, northwestern Alberta. *Bulleting of Canadian Petroleum Geology*, 39(2), 165–191.

Bjørlykke, K. & Høeg, K. (1997) Effects of burial diagenesis on stresses, compaction and fluid flow in sedimentary basins. *Marine and Petroleum Geology*, 14(3), 267–276. Available from: https://doi.org/10.1016/S0264-8172(96)00051-7

Boisvert, J.B., Manchuk, J.G. & Deutsch, C.V. (2009) Kriging in the presence of locally varying anisotropy using non-euclidean distances. *Mathematical Geosciences*, 41(5), 585–601. Available from: https://doi.org/10.1007/s11004-009-9229-1

Bourgeois, A., Joseph, P. & Lecomte, J.C. (2004) Three-dimensional full wave seismic modelling versus one-dimensional convolution: the seismic appearance of the Grès d'Annot turbidite system. *Geological Society Special Publication*, 221, 401–417. Available from: https://doi.org/10.1144/GSL.SP.2004.221.01.22

Cardiff, M. & Kitanidis, P.K. (2009) Bayesian inversion for facies detection: an extensible level set framework. *Water Resources Research*, 45(10). 1–15. Available from: https://doi.org/10.1029/2008WR007675

Červený, V. (2001) *Seismic ray theory*. Cambridge: Cambridge University Press.

Červený, V., Klimeš, L. & Pšenčík, I. (2007) Seismic ray method: Recent developments. *Advances in Geophysics*, 48, 1–126. Available from: https://doi.org/10.1016/S0065-2687(06)48001-8

Charvin, K., Hampson, G.J., Gallagher, K.L., Storms, J.E.A. & Labourdette, R. (2011) Characterization of controls on high-resolution stratigraphic architecture in wave-dominated shoreface–shelf parasequences using inverse numerical modeling. *Journal of Sedimentary Research*, 81(8), 562–578. Available from: https://doi.org/10.2110/JSR.2011.48

Chhoa, J.F. (2020) *An adaptive approach to Gibbs' Phenomenon*. Hattiesburg: University of Southern Mississippi.

Chilingar, G.V. (1964) Relationship between porosity, permeability, and grain-size distribution of sands and sandstones. *Developments in Sedimentology*, 1, 71–75. Available from: https://doi.org/10.1016/S0070-4571(08)70469-2

Cho, G.-C., Dodds, J. & Santamarina, J.C. (2006) Particle shape effects on packing density, stiffness, and strength: natural and crushed sands. *Journal of Geotechnical and Geoenvironmental Engineering*, 132(5), 591–602. Available from: https://doi.org/10.1061/(ASCE)1090-0241(2006)132:5(591)

Chopra, S., Castagna, J.P. & Portniaguine, O. (2006) Seismic resolution and thin-bed reflectivity inversion. *CSEG Recorder*, 31, 19–25. Available from: https://doi.org/10.1190/1.2369941

Cordua, K.S., Hansen, T.M. & Mosegaard, K. (2012) Monte Carlo full-waveform inversion of crosshole GPR data using multiple-point geostatistical a priori information. *Geophysics*, 77(2), H19–H31. Available from: https://doi.org/10.1190/geo2011-0170.1

Cox, D.R., Newton, A.M.W. & Huuse, M. (2020) An introduction to seismic reflection data: acquisition, processing and interpretation. In *Regional geology and tectonics: principles of geologic analysis*. Academic Press: Elsevier, pp. 571–603 Available from: https://doi.org/10.1016/B978-0-444-64134-2.00020-1

Crepaldi, J.L., de Figueiredo, L.P., Zerilli, A., Oliveira, I.S. & Sinnecker, J.P. (2024) Bayesian joint inversion of seismic and electromagnetic data for reservoir lithofluid facies, including geophysical and petrophysical rock properties. *Geophysics*, 89(3), K1–K16. Available from: https://doi.org/10.1190/geo2022-0546.1

Davydenko, M. (2016) *Full wavefield migration: seismic imaging using multiple scattering effects*. Delft: TU Delft. Available from: https://doi.org/10.4233/uuid:1cda75d5-8998-49fe-997e-b38c9b7f8b8b

Davydenko, M., & Verschuur, D. J. (2017). Full-wavefield estimation of angle-dependent reflectivity and migration velocity. *Proceedings of the 87th Annual International Meeting SEG*. 5631–5635.

de Jager, J. (2021) Handbook: *Risk and Volume Assessment*. Self-published.

Eberhart-Phillips, D., Han, D.H. & Zoback, M.D. (1989) Empirical relationships among seismic velocity, effective pressure, porosity, and clay content in sandstone. 54(1), 82–89. Available from: https://doi.org/10.1190/1.1442580

Fagin, S.W. (1991) *Seismic Modeling of Geologic Structures*. Society of Exploration Geophysicists. Available from: https://doi.org/10.1190/1.9781560802754

Falivene, O., Arbués, P., Ledo, J., Benjumea, B., Muñoz, J.A., Fernández, O. et al. (2010) Synthetic seismic models from outcrop-derived reservoir-scale three-dimensional facies models: the Eocene Ainsa turbidite system (southern Pyrenees). *AAPG Bulletin*, 94(3), 317–343. Available from: https://doi.org/10.1306/08030908157

Feng, R., Luthi, S.M., Gisolf, D. & Sharma, S. (2017) Obtaining a high-resolution geological and petrophysical model from the results of reservoir-orientated elastic wave-equation-based seismic inversion. *Petroleum Geoscience*, 23(3), 376–385. Available from: https://doi.org/10.1144/petgeo2015-076

Field, M.E. & Roy, P.S. (1984) Offshore transport and sand-body formation; evidence from a steep, high-energy shoreface, southeastern Australia. *Journal of Sedimentary Research*, 54(4), 1292–1302. Available from: https://doi.org/10.1306/212F85C1-2B24-11D7-8648000102C1865D

Folk, R.L. (1954) The distinction between grain size and mineral composition in sedimentary-rock nomenclature. *The Journal of Geology*, 62, 344–359.

Folk, R.L. & Ward, W.C. (1957) Brazos river bar [Texas]; a study in the significance of grain size parameters. *Journal of Sedimentary Research*, 27(1), 3–26. Available from: https://doi.org/10.1306/74D70646-2B21-11D7-8648000102C1865D

Fouedjio, F. (2017) Second-order non-stationary modeling approaches for univariate geostatistical data. *Stochastic Environmental Research and Risk Assessment*, 31(8), 1887–1906. Available from: https://doi.org/10.1007/s00477-016-1274-y

Friedman, G.M. (1962) On sorting, sorting coefficients, and the lognormality of the grain-size distribution of sandstones. *The Journal of Geology*, 70(6), 737–753. http://www.journals.uchicago.edu/t-and-c

Giles, M.R. (1997) Diagenesis: *a quantitative perspective*. Implications *for basin modelling and rock property prediction*. Berlin: Springer.

Gonzalez, E.F., Gesbert, S. & Hofmann, R. (2016) Adding geologic prior knowledge to Bayesian lithofluid facies estimation from seismic data. *Interpretation*, 4(3), SL1–SL8. Available from: https://doi.org/10.1190/INT-2015-0220.1

González, E.F., Mukerji, T. & Mavko, G. (2008) Seismic inversion combining rock physics and multiple-point geostatistics. *Geophysics*, 73(1), R11–R21. Available from: https://doi.org/10.1190/1.2803748

Grana, D. (2018) Joint facies and reservoir properties inversion. *Geophysics*, 83(3), M15–M24. Available from: https://doi.org/10.1190/geo2017-0670.1

Grana, D. (2019) Joint inversion of facies and reservoir properties. In 81st EAGE *conference and exhibition*, European Association of Geoscientists & Engineers.pp. 1–5. Available from: https://doi.org/10.3997/2214-4609.201901298

Granjeon, D. (2019) Use of high-performance stratigraphic forward modelling to improve siliciclastic and carbonate reservoir depositional architecture description. *Journal of the Japanese Association for Petroleum Technology*, 84(1), 59–70. Available from: https://doi.org/10.3720/japt.84.59

Granjeon, D. & Joseph, P. (1999) Concepts and applications of A 3-D multiple lithology, diffusive model in stratigraphic modeling. In *Nu*merical experiments in stratigraphy: recent advances in stratigraphic and sedimentologic computer simulations. SEPM Society for

Sedimentary Geology, Available from: https://doi.org/10.2110/PEC.99.62.0197

Grasseau, N., Grélaud, C., López-Blanco, M. & Razin, P. (2019) Forward seismic modeling as a guide improving detailed seismic interpretation of deltaic systems: example of the Eocene Sobrarbe delta outcrop (South-Pyrenean foreland basin, Spain), as a reference to the analogous subsurface Albian-Cenomanian Torok-Nanushuk Delta of the Colville Basin (NPRA, USA). *Marine and Petroleum Geology*, 100, 225–245. Available from: https://doi.org/10.1016/J.MARPETGEO.2018.11.010

Grippa, A., Hurst, A., Palladino, G., Iacopini, D., Lecomte, I. & Huuse, M. (2019) Seismic imaging of complex geometry: forward modeling of sandstone intrusions. *Earth and Planetary Science Letters*, 513, 51–63. Available from: https://doi.org/10.1016/j.epsl.2019.02.011

Hampson, G.J. & Storms, J.E.A. (2003) Geomorphological and sequence stratigraphic variability in wave-dominated, shoreface-shelf parasequences. *Sedimentology*, 50(4), 667–701. Available from: https://doi.org/10.1046/j.1365-3091.2003.00570.x

Han, D.H., Nur, A. & Morgan, D. (1986) Effects of porosity and clay content on wave velocities in sandstones. *Geophysics*, 51(11), 2093–2107. Available from: https://doi.org/10.1190/1.1442062

Harbaugh, J.W. (1993) Simulating sedimentary basins: an Overview of the SEDSIM model and its relevance to sequence stratigraphy. *Geoinformatics*, 4(3), 123–126.

Hodgetts, D. & Howell, J.A. (2000) Synthetic seismic modelling of a large-scale geological cross-section from the Book Cliffs, Utah, USA. *Petroleum Geoscience*, 6(3), 221–229. Available from: https://doi.org/10.1144/PETGEO.6.3.221

Holberg, O., Pajchel, J., Riste, P. & Helle, H.B. (1990) Comparison of ray tracing and finite-difference modeling. *SEG Technical Program Expanded Abstracts*, 1990, 1037–1041. Available from: https://doi.org/10.1190/1.1889901

Holgate, N.E., Hampson, G.J., Jackson, C.A.-L. & Petersen, S.A. (2014) Constraining uncertainty in interpretation of seismically imaged clinoforms in deltaic reservoirs, Troll field, Norwegian North Sea: insights from forward seismic models of outcrop analogs. *AAPG Bulletin*, 98(12), 2629–2663. Available from: https://doi.org/10.1306/05281413152

Holgate, N.E., Jackson, C.A.-L., Hampson, G.J. & Dreyer, T. (2015) Seismic stratigraphic analysis of the Middle Jurassic Krossfjord and Fensfjord formations, troll oil and gas field, northern North Sea. *Marine and Petroleum Geology*, 68, 352–380. Available from: https://doi.org/10.1016/j.marpetgeo.2015.08.036

Howell, J.A., Skorstad, A., MacDonald, A., Fordham, A., Flint, S., Fjellvoll, B. et al. (2008) Sedimentological parameterization of shallow-marine reservoirs. *Petroleum Geoscience*, 14(1), 17–34. Available from: https://doi.org/10.1144/1354-079307-787

Hubbert, M.K. & Rubey, W.W. (1959) Role of fluid pressure in mechanics of overthrust faulting: I. Mechanics of fluid-filled porous solids and its application to overthrust faulting. *GSA Bulletin*, 70(2), 115–166.

Jackson, A., Jackson, A., Stright, L., Hubbard, S.M. & Romans, B.W. (2019) Static connectivity of stacked deep-water channel elements constrained by high-resolution digital outcrop models. *AAPG Bulletin*, 103(12), 2943–2973. Available from: https://doi.org/10.1306/03061917346

Jackson, M.D., Hampson, G.J. & Sech, R.P. (2009) Three-dimensional modeling of a shoreface-shelf parasequence reservoir analog: part 2. Geologic controls on fluid flow and hydrocarbon recovery. *American Association of Petroleum Geologists Bulletin*, 93(9), 1183–1208. Available from: https://doi.org/10.1306/05110908145

Journel, A.G. (2005) Beyond covariance: the advent of multiple-point geostatistics. In *Geostatistics banff 2004*. Berlin: Springer, pp. 225–233. Available from: https://doi.org/10.1007/978-1-4020-3610-1_23

Jullum, M. & Kolbjørnsen, O. (2016) A Gaussian-based framework for local Bayesian inversion of geophysical data to rock properties. *Geophysics*, 81(3), R75–R87. Available from: https://doi.org/10.1190/geo2015-0314.1

Keen, T.R., Slingerland, R.L., Bentley, S.J., Furukawa, Y., Teague, W.J. & Dykes, J.D. (2012) Sediment transport on continental shelves: storm bed formation and preservation in heterogeneous sediments. *Sediments,* morphology and sedimentary processes on continental shelves: advances in technologies, research, and applications. Hoboken, NJ: Wiley, pp. 295–310. Available from: https://doi.org/10.1002/9781118311172.CH14

Kelly, K.R., Ward, R.W., Treitel, S. & Alford, R.M. (1976) Synthetic seismograms—a finite difference approach. *Geophysics*, 41(1), 2–27. Available from: https://doi.org/10.1190/1.1440605

Kemper, M. & Gunning, J. (2014) Joint impedance and facies inversion—seismic inversion redefined. *First Break*, 32(9), 89–95. Available from: https://doi.org/10.3997/1365-2397.32.9.77968

Ketzer, J.M., Morad, S., Evans, R. & Al-Aasm, I.S. (2002) Distribution of diagenetic alterations in fluvial, deltaic, and shallow marine sandstones within a sequence stratigraphic framework: evidence from the Mullaghmore formation (Carboniferous), NW Ireland. *Journal of Sedimentary Research*, 72(6), 760–774. Available from: https://doi.org/10.1306/042202720760

Klausen, T.G., Torland, J.A., Eide, C.H., Alaei, B., Olaussen, S. & Chiarella, D. (2018) Clinoform development and topset evolution in a mud-rich delta—the Middle Triassic Kobbe Formation, Norwegian Barents Sea. *Sedimentology*, 65(4), 1132–1169. Available from: https://doi.org/10.1111/sed.12417

Kumar, N. & Sanders, J.E. (1976) Characteristics of shoreface storm deposits; modern and ancient examples. *Journal of Sedimentary Research*, 46(1), 145–162. Available from: https://doi.org/10.1306/212F6EDD-2B24-11D7-8648000102C1865D

Laigle, L., Joseph, P., De Marsily, G. & Violette, S. (2013) 3-D process modelling of ancient storm-dominated deposits by an event-based approach: Application to Pleistocene-to-modern Gulf of Lions deposits. *Marine Geology*, 335, 177–199. Available from: https://doi.org/10.1016/j.margeo.2012.11.007

Lis, P. & Wysocka, A. (2012) Middle miocene deposits in carpathian foredeep: facies analysis and implications for hydrocarbon reservoir prospecting. *Annales Societatis Geologorum Poloniae*, 82, 239–253.

Liu, Y., Harding, A., Abriel, W. & Strebelle, S. (2004) Multiple-point simulation integrating wells, three-dimensional seismic data, and geology. *AAPG Bulletin*, 88(7), 905–921. Available from: https://doi.org/10.1306/02170403078

Liu, Y. & Sen, M.K. (2009) Advanced finite-difference methods for seismic modeling. *Geohorizons*, 14, 5–16.

Machuca-Mory, D.F. & Deutsch, C.V. (2013) Non-stationary geostatistical modeling based on distance weighted statistics and distributions. *Mathematical Geosciences*, 45(1), 31–48. Available from: https://doi.org/10.1007/s11004-012-9428-z

Madsen, O. (1991) Mechanics of cohesionless sediment transport in coastal waters. In *Proceedings of the Coastal Sediments*, ASCE. pp. 15–27.

Merletti, G.D. & Torres-Verdín, C. (2006) Accurate detection and spatial delineation of thin-sand sedimentary sequences via joint stochastic inversion of well logs and 3D Prestack seismic amplitude data. In Paper presented at the SPE annual technical conference and exhibition, San Antonio, Texas, USA. OnePetro. Available from: https://doi.org/10.2118/102444-MS

Merriman, R.J., Highley, D.E. & Cameron, D.G. (2003) *Definition and characteristics of very-fine grained sedimentary rocks : clay, mudstone, shale and slate*. Nottingham: British Geological Survey.

Mitchell, N.C. & Zhao, Z. (2023) Effects of currents and waves on the morphologies of coastal sandy clinoforms: sediment mobility calculations based on current meter and wave data from Southern California, U.S.A. *Journal of Sedimentary Research*, 93(7), 488–501. Available from: https://doi.org/10.2110/JSR.2023.002

Mur, A. & Waters, K. (2018) Play scale seismic characterization: using basin models as an input to seismic characterization in new and emerging plays. *SEG Technical Program Expanded Abstracts*, 2018, 555–559. Available from: https://doi.org/10.1190/segam2018-2992809.1

Neidell, N. S. (1986). Amplitude variation with offset. *The Leading Edge*, 5(3), 47–51.

Ostrander, W. J. (1984). Plane-wave reflection coefficients for gas sands at nonnormal angles of incidence. *Geophysics*, 49, 1637–1648.

Paola, C. (2000) Quantitative models of sedimentary basin filling. *Sedimentology*, 47, (Supplement 1), 121–178. Available from: https://doi.org/10.1046/J.1365-3091.2000.00006.X

Patro, B.C. & Sahu, B.K. (1974) Factor analysis of sphericity and roundness data of clastic quartz grains: environmental significance. *Sedimentary Geology*, 11(1), 59–78. Available from: https://doi.org/10.1016/0037-0738(74)90005-0

Pemberton, E.A.L., Stright, L., Fletcher, S. & Hubbard, S.M. (2018) The influence of stratigraphic architecture on seismic response: reflectivity modeling of outcropping deepwater channel units. *Interpretation*, 6(3), T783–T808. Available from: https://doi.org/10.1190/INT-2017-0170.1

Pendrel, J. & Schouten, H. (2020) Facies— the drivers for modern inversions. *The Leading Edge*, 39(2), 102–109. Available from: https://doi.org/10.1190/tle39020102.1

Picard, M.D. (1971) Classification of fine-grained sedimentary rocks. *Journal of Sedimentary Research*, 41(1), 179–195. Available from: https://doi.org/10.1306/74D7221B-2B21-11D7-8648000102C1865D

Pyrcz, M.J., McHargue, T., Clark, J., Sullivan, M. & Strebelle, S. (2012) Event-based geostatistical modeling: description and applications. In: Abrahamsen, P., Hauge, R., Kolbjørnsen, O. (Eds.) *Geostatistics oslo 2012. Quantitative geology and geostatistics*. Dordrecht: Springer, pp. 27–38. Available from: https://doi.org/10.1007/978-94-007-4153-9_3

Pyrcz, M.J., Sech, R.P., Covault, J.A., Willis, B.J., Sylvester, Z. & Sun, T. (2015) Stratigraphic rule-based reservoir modeling. *Bulletin of Canadian Petroleum Geology*, 63(4), 287–303. Available from: https://doi.org/10.2113/GSCPGBULL.63.4.287

Shuey, R. T. (1985). A simplification of the Zoeppritz equations. *Geophysics*, 50, 609–614.

Quiquerez, A., Allemand, P., Dromart, G. & Garcia, J. (2004) Impact of storms on mixed carbonate and siliciclastic shelves: insights from combined diffusive and fluid-flow transport stratigraphic forward model. *Basin Research*, 16(4), 431–449. Available from: https://www.academia.edu/23222459/Impact_of_storms_on_mixed_carbonate_and_siliciclastic_shelves_insights_from_combined_diffusive_and_fluid_flow_transport_stratigraphic_forward_model

Rabbel, O., Galland, O., Mair, K., Lecomte, I., Senger, K., Spacapan, J.B. et al. (2018) From field analogues to realistic seismic modelling: a case study of an oil-producing andesitic sill complex in the Neuquén Basin, Argentina. *Journal of the Geological Society*, 175(4), 580–593. Available from: https://doi.org/10.1144/JGS2017-116

Rawlinson, N., Hauser, J. & Sambridge, M. (2008) Seismic ray tracing and wavefront tracking in laterally heterogeneous media. *Advances in Geophysics*, 49, 203–273. Available from: https://doi.org/10.1016/S0065-2687(07)49003-3

Ringrose, P. & Bentley, M. (2015) *Reservoir model design: a practitioner's guide*. Berlin: Springer.

Rogers, J.J.W. & Head, W.B. (1961) Relationships between porosity, median size, and sorting coefficients of synthetic sands. *Journal of Sedimentary Petrology*, 31(3), 467–470.

Roncarolo, F. & Grana, D. (2010) Improved reservoir characterization integrating seismic inversion, rock physics model, and petroelastic log facies classification: a real case application. In: Proceedings of the SPE annual technical conference and exhibition, Florence, Italy, OnePetro. Available from: https://doi.org/10.2118/134919-MS

Rongier, G., Storms, J.E.A. & Cuesta Cano, A. (2023) *pyBarSim (Version 1). 4TU. ResearchData*. Software: https://github.com/grongier/pybarsim

Roy, P.S., Cowell, P.J., Ferland, M.A., Thom, B.G. & van de Plassche, O. (1995) Wave-dominated coasts. In *Coastal evolution: late quaternary shoreline morphodynamics*. Cambridge: Cambridge University Press, pp. 121–186.

Schön, J.H. (2011) Chapter 1–Rocks—their classification and general properties. In *Handbook of petroleum exploration and production*, vol. 8, Random Publications, pp. 1–16. Available from: https://doi.org/10.1016/S1567-8032(11)08001-3

Sclater, J.G. & Christie, P.A.F. (1980) Continental stretching: an explanation of the Post-Mid-Cretaceous subsidence of the central North Sea Basin. *Journal of Geophysical Research: Solid Earth*, 85(B7), 3711–3739. Available from: https://doi.org/10.1029/JB085iB07p03711

Sech, R.P., Jackson, M.D. & Hampson, G.J. (2009) Three-dimensional modeling of a shoreface-shelf parasequence reservoir analog: part 1. surface-based modeling to capture high-resolution fades architecture. *American Association of Petroleum Geologists Bulletin*, 93(9), 1155–1181. Available from: https://doi.org/10.1306/05110908144

Sheriff, R. E., & Geldart, L. P. (1995). Exploration Seismology. Cambridge University Press.

Shuster, M.W. & Aigner, T. (1994) Two-dimensional synthetic seismic and log cross sections from stratigraphic forward models. *AAPG Bulletin*, 78(3), 409–431. Available from: https://doi.org/10.1306/BDFF90C8-1718-11D7-8645000102C1865D

Simmons, M., Davies, A. & Cowliff, L. (2023) Plausible characterisation of subsurface geology is essential for the energy transition. *First Break*, 41(6), 69–74. Available from: https://doi.org/10.3997/1365-2397.fb2023045

Sømme, T.O., Howell, J.A., Hampson, G.J. & Storms, J.E.A. (2008) Genesis, architecture, and numerical modeling of intra-parasequence discontinuity surfaces in wave-dominated deltaic deposits: upper cretaceous sunnyside member, blackhawk formation, Book Cliffs, Utah, U.S.A. In *Recent advances in models of siliciclastic shallow-marine stratigraphy*. SEPM (Society for Sedimentary Geology), pp. 421–441. Available from: https://doi.org/10.2110/PEC.08.90.0421

Storms, J.E.A. (2003) Event-based stratigraphic simulation of wave-dominated shallow-marine environments. *Marine Geology*, 199(1–2), 83–100. Available from: https://doi.org/10.1016/S0025-3227(03)00144-0

Storms, J.E.A. & Hampson, G.J. (2005) Mechanisms for forming discontinuity surfaces within shoreface-shelf parasequences: sea level, sediment supply, or wave regime? *Journal of Sedimentary Research*, 75(1), 67–81. Available from: https://doi.org/10.2110/jsr.2005.007

Storms, J.E.A. & Swift, D.J.P. (2003) Shallow-marine sequences as the building blocks of stratigraphy: insights from numerical modelling. *Basin Research*, 15(3), 287–303. Available from: https://doi.org/10.1046/j.1365-2117.2003.00207.x

Storms, J.E.A., Weltje, G.J., Van Duke, J.J., Geel, C.R. & Kroonenberg, S.B. (2002) Process-response modeling of wave-dominated coastal systems: simulating evolution and stratigraphy on geological timescales. *Journal of Sedimentary Research*, 72(2), 226–239. Available from: https://doi.org/10.1306/052501720226

Suh, H.S., Kim, K.Y., Lee, J. & Yun, T.S. (2017) Quantification of bulk form and angularity of particle with correlation of shear strength and packing density in sands. *Engineering Geology*, 220, 256–265. Available from: https://doi.org/10.1016/j.enggeo.2017.02.015

Swift, D.J.P., Phillips, S. & Thorne, J.A. (1991) Sedimentation on continental margins, IV. Lithofacies and depositional systems. In Swift, D. J. P., Oertel, G. F., Tillman, R. W. & Thorne, J. A. (Eds.), *Shelf sand and sandstone bodies: geometry, facies and sequence stratigraphy*. vol. 14. Hoboken, NJ: Wiley, pp. 89–152

Tahir, S., Musta, B., Asis, J. & Hanis, F. (2018) Wave and tide influence in Neogene paralic hydrocarbon potential reservoirs in Sabah. *ASM Science Journal*, 11(2), 278–292.

Taylor, K.G., Gawthorpe, R.L., Curtis, C.D., Marshall, J.D. & Awwiller, D.N. (2000) Carbonate cementation in a sequence-stratigraphic framework: upper cretaceous sstones, book cliffs, Utah-Colorado. *Journal of Sedimentary Research*, 70(2), 360–372. Available from: https://doi.org/10.1306/2DC40916-0E47-11D7-8643000102C1865D

Tetzlaff, D.M. (2005) Modelling coastal sedimentation through geologic time. *Journal of Coastal Research*, 21((3), 610–617. Available from: https://doi.org/10.2112/04-704A.1

Tetzlaff, D.M. & Harbaugh, J.W. (1989) Simulating clastic sedimentation (computer methods in the geosciences) In: Tetzlaff, D. M. & Harbaugh, W. (Eds.). London: Van Nostrand Reinhold.

Tomasso, M., Bouroullec, R. & Pyles, D.R. (2010) The use of spectral recomposition in tailored forward seismic modeling of outcrop analogs. *AAPG Bulletin*, 94(4), 457–474. Available from: https://doi.org/10.1306/08240909051

Trask, P.D. (1930) Mechanical analysis of sediments by centrifuge. *Economic Geology*, 25(6), 581–599.

Tyler, N. & Finley, R.J. (1991) Architectural controls on the recovery of hydrocarbons from sandstone reservoers. In *The three-dimensional facies architecture of terrigenous clastic sediments and its implications for hydrocarbon discovery and recovery*. Tulsa: SEPM Society for Sedimentary Geology, pp. 1–5. Available from: https://doi.org/10.2110/csp.91.03.0001

Wan, L., Hurter, S., Bianchi, V., Li, P., Wang, J. & Salles, T. (2022) The roles and seismic expressions of turbidites and mass transport deposits using stratigraphic forward modeling and seismic forward modeling. *Journal of Asian Earth Sciences*, 232, 105110. Available from: https://doi.org/10.1016/j.jseaes.2022.105110

Wang, R., Jia, X. & Hu, T. (2004) The precise finite difference method for seismic modeling. *Applied Geophysics*, 1(2), 69–74. Available from: https://doi.org/10.1007/s11770-004-0001-5

Wendebourg, J. & Harbaugh, J.W. (1997) Chapter 4 Endowing simulated sequences with petrophysical flow properties. In Wendebourg, J. & Arbaugh, J.W. (Eds.) *Computer methods in the geosciences* vol. 16. Oxford: Pergamon, p. 81. Available from: https://doi.org/10.1016/S1874-561X(97)80005-3

Willis, B.J. & Tang, H. (2010) Three-dimensional connectivity of point-bar deposits. *Journal of Sedimentary Research*, 80(5), 440–454. Available from: https://archives.datapages.com/data/sepm/journals/080/080005/440_gsjsedres800440.htm

Yilmaz, Ö. (2001) *Seismic data analysis*. Houston, TX: Society of Exploration Geophysicists.

Zeng, H., Zhu, X. & Zhu, R. (2013) New insights into seismic stratigraphy of shallow-water progradational sequences: subseismic clinoforms. *Interpretation*, 1(1), SA35–SA51. Available from: https://doi.org/10.1190/INT-2013-0017.1

## SUPPORTING INFORMATION

Additional supporting information can be found online in the Supporting Information section at the end of this article.

**How to cite this article:** Cuesta Cano, A., Karimzadanzabi, A., Storms, J.E.A., Rongier, G., Verschuur, D.J. & Martinius, A.W. (2025) Discretization of small-scale, stratigraphic heterogeneities and its impact on the seismic response: Lessons from the application of process-based modelling. *Geophysical Prospecting*, 73, 1280–1300. https://doi.org/10.1111/1365-2478.70015